A priori tests of subgrid-scale models in an anisothermal turbulent channel flow at low mach number

Dorian Dupuy, Adrien Toutant, Françoise Bataille

A priori tests of subgrid-scale models in an anisothermal turbulent channel flow at low Mach number

Dorian Dupuy[1], Adrien Toutant*[1], and Françoise Bataille[1]

[1]*PROMES CNRS, Université de Perpignan Via Domitia, Rambla de la thermodynamique, Tecnosud, 66100 Perpignan, France*

(Published version: International Journal of Thermal Sciences 145, 105999 (2019); https://doi.org/10.1016/j.ijthermalsci.2019.105999)

Abstract

The subgrid-scale modelling of a low Mach number strongly anisothermal turbulent flow is investigated using direct numerical simulations. The study is based on the filtering of the low Mach number equations, suited to low Mach number flows with highly variable fluid properties. The results are relevant to formulations of the filtered low Mach number equations established with the classical filter or the Favre filter. The two most significant subgrid terms of the filtered low Mach number equations are considered. They are associated with the momentum convection and the density-velocity correlation. We focus on eddy-viscosity and eddy-diffusivity models. Subgrid-scale models from the literature are analysed and two new models are proposed. The subgrid-scale models are compared to the exact subgrid term using the instantaneous flow field of the direct numerical simulation of a strongly anisothermal fully developed turbulent channel flow. There is no significant differences between the use of the classical and Favre filter regarding the performance of the models. We suggest that the models should take into account the asymptotic near-wall behaviour of the filter length. Eddy-viscosity and eddy-diffusivity models are able to represent the energetic contribution of the subgrid term but not its effect in the flow governing equations. The AMD and scalar AMD models are found to be in better agreement with the exact subgrid terms than the other investigated models in the a priori tests.

1 Introduction

This paper addresses the large-eddy simulation subgrid-scale modelling of low Mach number strongly anisothermal turbulent flows. Flows subjected to a strong temperature gradient are prevalent in many industrial processes, such as heat exchangers, propulsion systems or solar power towers [48]. They are characterised by strong coupling between turbulence and temperature, along with high variations of the fluid properties (density, viscosity and thermal conductivity) with temperature [52, 3, 19]. In many cases, the direct numerical simulation (DNS) of strongly anisothermal turbulent flows is unpracticable because too many scales of temperature and velocity are produced and not enough resolution is available to resolve all the relevant scales. In order to predict the large-scale behaviour of low Mach number strongly anisothermal turbulent flows, thermal large-eddy simulation (LES) is an effective alternative. Large-eddy simulation is based on the explicit resolution of the large scales of turbulence and the use of subgrid-scale models to account for the

*Corresponding author : adrien.toutant@univ-perp.fr

effect of the smaller scales on the large scales. The scale separation may be represented by the application of a low-pass spatial filter on the flow governing equations.

The filtering of the low Mach number equations gives rise to specific subgrid terms. Using a priori tests, Dupuy *et al.* [18] assessed the amplitude of all subgrid terms in several formulations. The expression of the filtered low Mach equations with the unweighted classical filter and the density-weighted Favre filter [20] leads to two different set of equations involving the same non-negligible subgrid terms [16, 17, 18]. The two most significant subgrid terms are associated with the momentum convection and the density-velocity correlation. The adequate modelling of these subgrid terms is required for the large-eddy simulation of low Mach number strongly anisothermal turbulent flows.

Various modelling strategies have been devised to represent the subgrid terms. Two main types of model are found: structural models, established with no prior knowledge of the nature of the effect of the subgrid term, and functional models, which assume that the effect of the subgrid term is similar to molecular diffusion and therefore acts as a dissipative action [46]. The subgrid-scale models should be consistent with important mathematical and physical properties of the Navier–Stokes equations and the turbulent stresses [49]. With regard to the subgrid term associated with momentum convection, the functional eddy-viscosity models are by far the most used because they are simple, inexpensive and robust. A review of eddy-viscosity models may be found in [46, 56, 49]. The eddy-viscosity assumption can be extended to the density-velocity correlation subgrid term using the constant subgrid-scale Prandtl or Schmidt number assumption. This is referred to as eddy-diffusivity models.

In this paper, we assess the subgrid-scale models a priori using the flow field from the direct numerical simulation of a strongly anisothermal turbulent channel flow. In the literature, a priori studies of the subgrid-scale models have been carried out in incompressible flows [14, 1, 32, 41, 28], passive and active scalar decaying homogeneous turbulence [13, 23] and in flows with purely compressible effects, in a temporal shear layer [60, 61, 59], a multi-species mixing layer [6], and in freely decaying homogeneous isotropic turbulence [34]. Besides, there are several works in the literature dealing with the large-eddy simulation of multiphase flows [8, 11, 33, 39, 43, 62, 21, 64]. A priori tests have been carried out for two-phase divergence-free flows [53, 54, 55, 25]. The analysis is here extended to low Mach number strongly anisothermal turbulent flows. We focus on eddy-viscosity and eddy-diffusivity models. Structural models, such as the scale-similarity [4] and gradient model [27], are known to display high degrees of correlation with the exact subgrid term in a priori tests despite easily leading to instabilities when used in an actual large-eddy simulation [4, 46, 47, 5, 25]. Eddy-viscosity models, which assume that the subgrid term is aligned with the rate of deformation tensor or the scalar gradient, are purely dissipative and have desirable property for numerical stability. Besides, by restricting the study to a single family of models, we may hope that the a priori tests have a more easy-to-interpret relevance for a posteriori results. The subgrid-scale models investigated are the Smagorinsky model [50], the WALE model [36], the Vreman model [58], the Sigma model [37], the AMD model [44], the scalar AMD model [2], the VSS model [45] and the Kobayashi model [26]. In addition, two new eddy-viscosity and eddy-diffusivity models are proposed and investigated, the Anisotropic Smagorinsky model, which attempts to improve anisotropy of the Smagorinsky model by involving three filter length scales instead of one, and the MMG model, which may be viewed as multiplicative mixed model.

The filtering of the low Mach number equations is described in section 2. The subgrid-scale models are presented in section 3. The channel flow configuration and the numerical

method are given in section 4. The section 5 discusses the asymptotic near-wall behaviour of the models. The results are analysed in section 6.

2 Filtering of the low Mach number equations

The low Mach number equations are an approximation of the Navier–Stokes equations suited to turbulent flows with a low Mach number ($Ma < 0.3$) but subjected to large variations of the fluid properties. Using Paolucci's method [38], each variable of the Navier–Stokes equations is written as a power series of the squared Mach number. Neglecting all but the smaller-order terms, the pressure is split in two parts: The thermodynamical pressure P (constant in space), which represents the mean pressure in the domain, and the mechanical pressure P_0, associated with the momentum variations. The resulting equations are free from acoustic waves.

Considering in addition an ideal gas and neglecting gravity, the low Mach number equations are given by:

- Mass conservation equation
$$\frac{\partial \rho}{\partial t} + \frac{\partial \rho U_j}{\partial x_j} = 0, \tag{1}$$

- Momentum conservation equation
$$\frac{\partial \rho U_i}{\partial t} = -\frac{\partial \rho U_j U_i}{\partial x_j} - \frac{\partial P}{\partial x_i} + \frac{\partial \Sigma_{ij}(\boldsymbol{U}, T)}{\partial x_j}, \tag{2}$$

- Energy conservation equation
$$\frac{\partial U_j}{\partial x_j} = -\frac{1}{\gamma P_0}\left[(\gamma - 1)\frac{\partial Q_j(T)}{\partial x_j} + \frac{\partial P_0}{\partial t}\right], \tag{3}$$

- Ideal gas law
$$T = \frac{P_0}{\rho r}, \tag{4}$$

with ρ the density, T the temperature, $\Sigma_{ij}(\boldsymbol{U}, T)$ the shear-stress tensor, $Q_j(T)$ the conductive heat flux, γ the heat capacity ratio, r the ideal gas specific constant, t the time, P the mechanical pressure, P_0 the thermodynamical pressure, U_i the i-th component of velocity and x_i the Cartesian coordinate in i-th direction. Einstein summation convention is used. The low Mach number equations impose the local energy conservation by a constraint (3) on the divergence of the velocity [35].

The filtering of the low Mach number equations may lead to different formulations of the filtered low Mach number equations depending on the variables we express the equations with and the manner the equations are arranged upon filtering. Two formulations of the filtered low Mach number equations are selected, the Velocity formulation and the Favre formulation. In the Velocity formulation, a spatial filter ($\overline{\cdot}$, classical filter) is applied on the low Mach number equations with the momentum conservation equation rewritten as the velocity transport equation. The equations are then expressed in terms of classical-filtered variables. The Favre formulation is based on the use of a density-weighted filter ($\widetilde{\cdot}$, Favre filter), defined for any ϕ, as $\widetilde{\phi} = \overline{\rho\phi}/\overline{\rho}$. In the Favre formulation, the low

Mach number equations are filtered with the classical filter and expressed in terms of Favre-filtered variables.

Retaining only the most significant subgrid terms [16, 17, 18], the filtered low Mach number equations are given in the Velocity formulation by:

$$\frac{\partial \overline{\rho}}{\partial t} + \frac{\partial}{\partial x_j}\left(\overline{\rho}\overline{U}_j + F_{\rho U_j}\right) = 0, \tag{5}$$

$$\frac{\partial \overline{U}_i}{\partial t} = -\frac{\partial}{\partial x_j}\left(\overline{U}_j\,\overline{U}_i + F_{U_jU_i}\right) + \overline{U}_i\frac{\partial \overline{U}_j}{\partial x_j} - \frac{1}{\overline{\rho}}\frac{\partial \overline{P}}{\partial x_i} + \frac{1}{\overline{\rho}}\frac{\partial \Sigma_{ij}(\overline{\boldsymbol{U}},\overline{T})}{\partial x_j}, \tag{6}$$

$$\frac{\partial \overline{U}_j}{\partial x_j} = -\frac{1}{\gamma P_0}\left[(\gamma-1)\frac{\partial Q_j(\overline{T})}{\partial x_j} + \frac{\partial P_0}{\partial t}\right], \tag{7}$$

$$\overline{T} = \frac{P_0}{r\overline{\rho}}, \tag{8}$$

and in the Favre formulation by:

$$\frac{\partial \overline{\rho}}{\partial t} + \frac{\partial \overline{\rho}\widetilde{U_j}}{\partial x_j} = 0, \tag{9}$$

$$\frac{\partial \overline{\rho}\widetilde{U}_i}{\partial t} = -\frac{\partial}{\partial x_j}\left(\overline{\rho}\widetilde{U}_j\widetilde{U}_i + \overline{\rho}G_{U_jU_i}\right) - \frac{\partial \overline{P}}{\partial x_i} + \frac{\partial \Sigma_{ij}(\widetilde{\boldsymbol{U}},\widetilde{T})}{\partial x_j}, \tag{10}$$

$$\frac{\partial}{\partial x_j}\left(\widetilde{U}_j + \overline{\rho}G_{U_j/\rho}\right) = -\frac{1}{\gamma P_0}\left[(\gamma-1)\frac{\partial Q_j(\widetilde{T})}{\partial x_j} + \frac{\partial P_0}{\partial t}\right], \tag{11}$$

$$\widetilde{T} = \frac{P_0}{\overline{\rho}r}, \tag{12}$$

with the subgrid terms:

$$F_{U_jU_i} = \overline{U_jU_i} - \overline{U}_j\,\overline{U}_i \tag{13}$$

$$G_{U_jU_i} = \widetilde{U_jU_i} - \widetilde{U}_j\widetilde{U}_i \tag{14}$$

$$F_{\rho U_j} = \overline{\rho U_j} - \overline{\rho}\overline{U}_j \tag{15}$$

$$G_{U_j/\rho} = \widetilde{U_j/\rho} - \widetilde{U}_j/\overline{\rho} \tag{16}$$

The Velocity and Favre formulations both involve a subgrid term associated with the momentum convection, $F_{U_jU_i}$ or $G_{U_jU_i}$, and a subgrid term associated with the density-velocity correlation, $F_{\rho U_j}$ or $G_{U_j/\rho}$, such that

$$\frac{F_{\rho U_j}}{\overline{\rho}} = -\overline{\rho}G_{U_j/\rho}. \tag{17}$$

The use of the Favre filter removes the need for the modelling of the density-velocity correlation from the mass conservation equation but requires the modelling of an additional subgrid term in the energy conservation equation [16, 17, 18].

The fluid (air) is assumed to be Newtonian to compute the shear-stress tensor,

$$\Sigma_{ij}(\boldsymbol{U},T) = \mu(T)\left(\frac{\partial U_i}{\partial x_j} + \frac{\partial U_j}{\partial x_i}\right) - \frac{2}{3}\mu(T)\frac{\partial U_k}{\partial x_k}\delta_{ij}, \tag{18}$$

with $\mu(T)$ the dynamic viscosity and δ_{ij} the Kronecker delta. The heat flux is given by

$$Q_j(T) = -\lambda(T)\frac{\partial T}{\partial x_j}, \tag{19}$$

with $\lambda(T)$ the thermal conductivity. The variations of viscosity with temperature are accounted for by Sutherland's law [51],

$$\mu(T) = \mu_0 \left(\frac{T}{T_0}\right)^{\frac{3}{2}} \frac{T_0 + S}{T + S}, \tag{20}$$

with $\mu_0 = 1.716 \cdot 10^{-5}$ Pa s, $S = 110.4$ K and $T_0 = 273.15$ K. The conductivity is deduced from the Prandlt number Pr and the heat capacity at constant pressure C_p, both assumed constant with $Pr = 0.76$ and $C_p = 1005$ J kg^{-1} K^{-1}. The ideal gas specific constant is $r = 287$ J kg^{-1} K^{-1}.

3 Subgrid-scale models

The subgrid terms of the Velocity and Favre formulations are formally similar. Accordingly, the same modelling procedure is used in both cases. To formalise this, we may express the subgrid-scale models as a function of the filter length scales and of the filtered velocity and density in the two formulations:

$$F_{U_jU_i} \approx \tau_{ij}^{\mathrm{mod}}(\overline{\boldsymbol{U}}, \overline{\boldsymbol{\Delta}}), \tag{21}$$

$$G_{U_jU_i} \approx \tau_{ij}^{\mathrm{mod}}(\widetilde{\boldsymbol{U}}, \overline{\boldsymbol{\Delta}}), \tag{22}$$

$$F_{\rho U_j} \approx \pi_{j}^{\mathrm{mod}}(\overline{\boldsymbol{U}}, \overline{\rho}, \overline{\boldsymbol{\Delta}}), \tag{23}$$

$$G_{U_j/\rho} \approx \pi_{j}^{\mathrm{mod}}(\widetilde{\boldsymbol{U}}, 1/\overline{\rho}, \overline{\boldsymbol{\Delta}}), \tag{24}$$

where the functions $\tau_{ij}^{\mathrm{mod}}(\boldsymbol{U}, \overline{\boldsymbol{\Delta}})$ and $\pi_{j}^{\mathrm{mod}}(\boldsymbol{U}, \phi, \overline{\boldsymbol{\Delta}})$ are model-dependent but do not depend on the formulation.

Eddy-viscosity models for the subgrid term associated with momentum convection may be written in the form

$$\tau_{ij}^{\mathrm{mod}}(\boldsymbol{U}, \overline{\boldsymbol{\Delta}}) = -2\nu_e^{\mathrm{mod}}(\boldsymbol{g}, \overline{\boldsymbol{\Delta}}) S_{ij}, \tag{25}$$

with $S_{ij} = \frac{1}{2}\left(g_{ij} + g_{ji}\right)$ the rate of deformation tensor and $\boldsymbol{g}$ the velocity gradient, defined by $g_{ij} = \partial_j \tilde{U}_i$. Notice that $\tau_{ij}^{\mathrm{mod}}(\boldsymbol{U}, \overline{\boldsymbol{\Delta}})$ may be considered traceless without loss of generality, even in the incompressible case, since the trace can be included as part of the filtered pressure $\overline{P}$. The eddy-viscosity $\nu_e^{\mathrm{mod}}(\boldsymbol{g}, \overline{\boldsymbol{\Delta}})$ is given by the model used. The following models from the literature are investigated in this paper using a priori tests:

Smagorinsky model [50]:
$$\nu_e^{\mathrm{Smag.}}(\boldsymbol{g}, \overline{\boldsymbol{\Delta}}) = \left(C^{\mathrm{Smag.}}\overline{\Delta}\right)^2 |\boldsymbol{S}|, \tag{26}$$

WALE model [36]:
$$\nu_e^{\mathrm{WALE}}(\boldsymbol{g}, \overline{\boldsymbol{\Delta}}) = \left(C^{\mathrm{WALE}}\overline{\Delta}\right)^2 \frac{\left(\mathcal{S}_{ij}^d \mathcal{S}_{ij}^d\right)^{\frac{3}{2}}}{\left(S_{mn}S_{mn}\right)^{\frac{5}{2}} + \left(\mathcal{S}_{mn}^d \mathcal{S}_{mn}^d\right)^{\frac{5}{4}}}, \tag{27}$$

Vreman model [58]:
$$\nu_e^{\mathrm{Vreman}}(\boldsymbol{g}, \overline{\boldsymbol{\Delta}}) = C^{\mathrm{Vreman}} \sqrt{\frac{\mathrm{II}_G}{g_{mn}g_{mn}}}, \tag{28}$$

Sigma model [37]:
$$\nu_e^{\mathrm{Sigma}}(\boldsymbol{g}, \overline{\boldsymbol{\Delta}}) = \left(C^{\mathrm{Sigma}}\overline{\Delta}\right)^2 \frac{\sigma_3\left(\sigma_1 - \sigma_2\right)\left(\sigma_2 - \sigma_3\right)}{\sigma_1^2}, \tag{29}$$

AMD model [44]:
$$\nu_e^{\mathrm{AMD}}(\boldsymbol{g}, \overline{\boldsymbol{\Delta}}) = C^{\mathrm{AMD}} \frac{\max(0, -G_{ij}S_{ij})}{g_{mn}g_{mn}}, \tag{30}$$

VSS model [45]: $$\nu_e^{\mathrm{VSS}}(\boldsymbol{g},\overline{\boldsymbol{\Delta}}) = \left(C^{\mathrm{VSS}}\overline{\Delta}\right)^2 \frac{(R_{ij}R_{ij})^{\frac{3}{2}}}{(S_{mn}S_{mn})^{\frac{5}{2}}}, \tag{31}$$

Kobayashi model [26]: $$\nu_e^{\mathrm{Koba.}}(\boldsymbol{g},\overline{\boldsymbol{\Delta}}) = C^{\mathrm{Koba.}}\overline{\Delta}^2 \left|F_g\right|^{\frac{3}{2}} (1-F_g)\left|\boldsymbol{S}\right|, \tag{32}$$

where $|\boldsymbol{S}| = \sqrt{2S_{ij}S_{ij}}$ is a norm of $\boldsymbol{S}$, $\mathcal{S}_{ij}^d = \frac{1}{2}\left(g_{ik}g_{kj}+g_{jk}g_{ki}\right) - \frac{1}{3}g_{kp}g_{pk}\delta_{ij}$ the traceless symmetric part of the squared velocity gradient tensor, $\sigma_1 \geq \sigma_2 \geq \sigma_3$ the three singular values of $\boldsymbol{g}$, $G_{ij} = \overline{\Delta}_k^2 g_{ik}g_{jk}$ the gradient model for the subgrid term associated with momentum convection [27], $\mathrm{II}_G = \frac{1}{2}\left(\mathrm{tr}^2\left(G\right) - \mathrm{tr}\left(G^2\right)\right)$ its second invariant, $R_{ij} = \beta_i g_{jj}$ the volumetric strain-stretching, with $\beta = (S_{23}, S_{13}, S_{12})$, and $F_g = \left(\Omega_{ij}\Omega_{ij} - S_{ij}S_{ij}\right) / \left(\Omega_{mn}\Omega_{mn} + S_{mn}S_{mn}\right)$ the coherent structure function, with $\Omega_{ij} = \frac{1}{2}\left(g_{ij} - g_{ji}\right)$ the spin tensor or rate of rotation tensor. Only constant coefficient versions of eddy-viscosity and eddy-diffusivity models are considered. The typical value of the coefficients from the literature is $C^{\mathrm{Smag.}} = 0.10$, $C^{\mathrm{WALE}} = 0.55$, $C^{\mathrm{Vreman}} = 0.07$, $C^{\mathrm{Sigma}} = 1.5$, $C^{\mathrm{AMD}} = 0.3$, $C^{\mathrm{VSS}} = 1.3$ and $C^{\mathrm{Koba.}} = 0.045$. The corresponding dynamic versions of these models are not considered in order to assess the relevance of the models before any dynamic correction [22, 29, 40]. The filter length scale is computed following Deardorff [15] as $\overline{\Delta} = (\overline{\Delta}_x\overline{\Delta}_y\overline{\Delta}_z)^{1/3}$. A review of alternative possible definitions may be found in Trias *et al.* [57].

Following the same rationale, eddy-diffusivity models for the density-velocity correlation subgrid term may be written in the form

$$\pi_j^{\mathrm{mod}}(\boldsymbol{U},\phi,\overline{\boldsymbol{\Delta}}) = -2\kappa_e^{\mathrm{mod}}(\boldsymbol{g},\boldsymbol{d},\overline{\boldsymbol{\Delta}})d_j. \tag{33}$$

with $\boldsymbol{d}$ the scalar gradient, defined by $d_j = \partial_j\phi$. It is common to express the eddy-diffusivity $\kappa_e^{\mathrm{mod}}(\boldsymbol{g},\overline{\boldsymbol{\Delta}})$ using the constant subgrid-scale Prandtl or Schmidt number assumption,

$$\kappa_e^{\mathrm{mod}}(\boldsymbol{g},\boldsymbol{d},\overline{\boldsymbol{\Delta}}) = \frac{1}{Pr_t}\nu_e^{\mathrm{mod}}(\boldsymbol{g},\overline{\boldsymbol{\Delta}}), \tag{34}$$

where Pr_t is the subgrid-scale Prandtl or Schmidt number. This provide a corresponding eddy-diffusivity model for each eddy-viscosity of equations (26–32). The dimensionless number Pr_t corresponds to a subgrid-scale Schmidt number in the Velocity formulation and a subgrid-scale Prandtl number in the Favre formulation. Given the formal similarity between the density-velocity correlation subgrid term in the Velocity and Favre formulation and the ideal gas law (4) which relates density and temperature, it is presumed that the same value may be used in the two formulations. Alternatively, some specific eddy-diffusivity models have been suggested in the literature [23, 2]. We investigate using a priori tests the eddy-diffusivity models associated with equations (26–32) and the following specific model:

Scalar AMD model [2]: $$\kappa_e^{\mathrm{SAMD}}(\boldsymbol{g},\boldsymbol{d},\overline{\boldsymbol{\Delta}}) = C^{\mathrm{SAMD}}\frac{\max(0,-D_jd_j)}{d_md_m}, \tag{35}$$

with $D_j = \overline{\Delta}_k^2 g_{jk}d_k$ the gradient model for the density-velocity correlation subgrid term.

In addition, we devised two new eddy-viscosity and eddy-diffusivity models for the purpose of this study. First, the Anisotropic Smagorinsky model is a modified version of the Smagorinsky model, associated with a single filter length scale, devised to involve the three filter length scales. This aims to improve the anisotropy of the model. The model is obtained by substituting in equations (25) and (33) the velocity gradient $\boldsymbol{g}$ and respectively

the scalar gradient $\boldsymbol{d}$ by the scaled velocity gradient $\boldsymbol{g^a}$, defined by $g^a_{ij} = (\overline{\Delta}_j/\overline{\Delta})\partial_j U_i$, and respectively the scaled scalar gradient $\boldsymbol{d^a}$, defined by $d^a_j = (\overline{\Delta}_j/\overline{\Delta})\partial_j \phi$. Namely,

$$\tau_{ij}^{\text{An.Smag.}}(\boldsymbol{U}, \overline{\boldsymbol{\Delta}}) = -2\nu_e^{\text{Smag.}}(\boldsymbol{g^a}, \overline{\boldsymbol{\Delta}}) S^a_{ij}, \tag{36}$$

$$\pi_{j}^{\text{An.Smag.}}(\boldsymbol{U}, \phi, \overline{\boldsymbol{\Delta}}) = -2\kappa_e^{\text{Smag.}}(\boldsymbol{g^a}, \boldsymbol{d^a}, \overline{\boldsymbol{\Delta}}) d^a_j, \tag{37}$$

with $S^a_{ij} = \frac{1}{2}\left(g^a_{ij} + g^a_{ji}\right)$ the scaled rate of deformation tensor. The eddy-viscosity and eddy-diffusivity are computed using equations (26) and (34). A similar procedure could be applied to obtain an anisotropic version of the WALE, Sigma, VSS and Kobayashi models.

Besides, we study the multiplicative mixed model based on the gradient model (MMG model), a functional model constructed such that its magnitude is determined by the gradient model [27] and its orientation is aligned with the rate of deformation tensor or the scalar gradient depending on the subgrid term. This procedure is reminiscent of the multiplicative mixed model of Ghaisas and Frankel [23, 24] which had an opposite purpose. The eddy-viscosity and eddy-diffusivity according to the MMG model are given by,

MMG model:
$$\nu_e^{\text{MMG}}(\boldsymbol{g}, \overline{\boldsymbol{\Delta}}) = -C^{\text{MMG}} \frac{G_{kk}}{|\boldsymbol{S}|}, \tag{38}$$

Scalar MMG model:
$$\kappa_e^{\text{SMMG}}(\boldsymbol{g}, \boldsymbol{d}, \overline{\boldsymbol{\Delta}}) = -C^{\text{SMMG}} \frac{\sqrt{D_i D_i}}{\sqrt{d_m d_m}}. \tag{39}$$

A similar procedure can be applied to other structural models, such as the scale-similarity model [4]. We may also view the MMG model as a multiplicative mixed model. Using the the Smagorinsky model and the isotropic part modelling of Yoshizawa [63],

$$\tau_{mm}^{\text{Yosh.}}(\boldsymbol{U}, \overline{\boldsymbol{\Delta}}) = 2C^{\text{Yosh.}} \overline{\Delta}^2 \left|\boldsymbol{S}\right|^2, \tag{40}$$

the MMG model $\tau_{ij}^{\text{MMG}}(\boldsymbol{U}, \overline{\boldsymbol{\Delta}}) = -2\nu_e^{\text{MMG}}(\boldsymbol{g}, \overline{\boldsymbol{\Delta}}) S_{ij}$ can be reformulated as

$$\tau_{ij}^{\text{MMG}}(\boldsymbol{U}, \overline{\boldsymbol{\Delta}}) = G_{kk} \frac{\tau_{ij}^{\text{Smag.}}(\boldsymbol{U}, \overline{\boldsymbol{\Delta}})}{\tau_{mm}^{\text{Yosh.}}(\boldsymbol{U}, \overline{\boldsymbol{\Delta}})} \tag{41}$$

emphasising that the MMG model combines the magnitude of the gradient model and the structure of the Smagorinsky model. This leads by identification $C^{\text{MMG}} = (C^{\text{Smag.}})^2/(2C^{\text{Yosh.}})$. Note that the Vreman, AMD and scalar AMD models also directly involve the gradient model [27].

4 Numerical study configuration

4.1 Channel flow configuration

We consider a fully developed three-dimensional anisothermal channel flow, as represented in figure 1. This geometry is one of the simpler that reproduces the distinctive features of low Mach number strongly anisothermal turbulent flows. The channel is periodic in the streamwise (x) and spanwise (z) directions. The wall-normal direction is denoted (y). The domain size is $4\pi h \times 2h \times 2\pi h$, with $h = 15$ mm. The temperature at the channel walls is imposed at $T_1 = 293$ K at the cold wall ($y = 0$) and $T_2 = 586$ K at the hot wall ($y = 2h$). This creates a temperature gradient in the wall-normal direction.

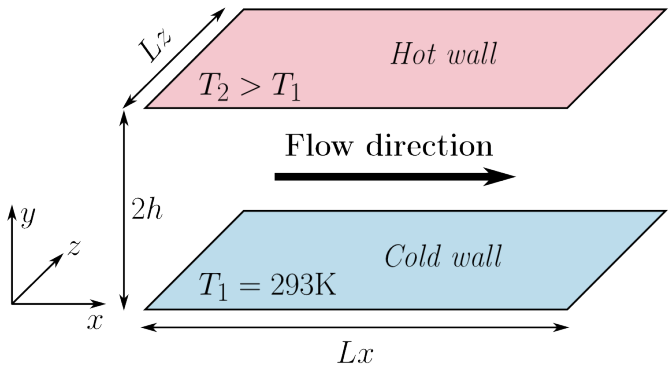

Figure 1 – Biperiodic anisothermal channel flow.

The mean friction Reynolds number is $Re_\tau = 180$, where Re_τ is defined as the average of the friction Reynolds numbers $Re_{\tau,\omega}$ calculated at the hot and cold wall,

$$Re_{\tau,\omega} = \frac{U_\tau h}{\nu_\omega}, \tag{42}$$

with $U_\tau = \nu_\omega (\partial_y \overline{U}_x)_\omega^{0.5}$ the friction velocity and ν_ω the wall kinematic viscosity.

4.2 Numerical settings

The mesh contains $384 \times 266 \times 384$ grid points and is regular in the homogeneous directions. It follows a hyperbolic tangent law in the wall-normal coordinate direction. The wall-normal grid coordinates are symmetrical with respect to the plane $y = h$. In the first half of the channel, they are given by

$$y_k = h\left(1 + \frac{1}{a}\tanh\left[\left(\frac{k-1}{N_y - 1} - 1\right)\tanh^{-1}(a)\right]\right), \tag{43}$$

with $a = 0.97$ the mesh dilatation parameter and N_y the number of grid points in the wall-normal direction. The cell sizes in wall units are $\Delta_x^+ = 8.5$, $\Delta_y^+ = 0.13$ at the wall and 4.2 at the centre of the channel and $\Delta_z^+ = 4.2$. A finite volume method is used with a third-order Runge–Kutta time scheme and a fourth-order centred momentum convection scheme. This is performed using the TrioCFD software [9].

4.3 Filtering process

The subgrid terms and the models are computed from the filtering of the instantaneous DNS data at the resolution of a large-eddy simulation mesh. The filter corresponds to a mesh with $48 \times 50 \times 48$ grid points ($\Delta_x^+ = 68$; $\Delta_y^+ = 0.5$ – 25; $\Delta_z^+ = 34$) constructed as the DNS mesh. Due to the inhomogeneity of the mesh, the filter width is variable in the wall-normal direction.

A top-hat filter is used. In one dimension, it is given in the physical space by

$$\overline{\psi}(x) = \frac{1}{\overline{\Delta}(x)} \int_{x-\frac{1}{2}\overline{\Delta}(x)}^{x+\frac{1}{2}\overline{\Delta}(x)} \psi(\xi) d\xi. \tag{44}$$

Multidimensional filtering is carried out by sequentially applying the one-dimensional filter in the three spatial directions. In order to carry out the filtering with an arbitrary filter length, the DNS data are first interpolated using a cubic spline. The top-hat filter is then computed from the interpolated value without mesh restrictions.

The discretisation of the differential operator of the models is carried out on the DNS grid, thus using data not available in an a posteriori large-eddy simulation [31]. This assesses the relevance of the models without regard to numerical errors. The data from 100 uncorrelated timesteps were averaged in order to obtain a satisfactory convergence of the results.

5 Asymptotic near-wall behaviour of the models

The WALE, Sigma, VSS and Kobayashi models have been designed to have an eddy-viscosity with a proper asymptotic near-wall behaviour for the subgrid term associated with momentum convection. While the components of the subgrid terms have different wall orders, the preferable asymptotic near-wall behaviour of the eddy-viscosity is cubic with respect to the distance to the wall, that is $\nu_e^{\mathrm{mod}}(\boldsymbol{g}, \overline{\boldsymbol{\Delta}})\big|_\omega = \mathcal{O}(y^3)$. A reason is that it is the order that the eddy-viscosity should have for the near-wall behaviour of the subgrid kinetic energy dissipation to be consistent with the exact subgrid kinetic energy dissipation. The asymptotic near-wall behaviour of the models given in the literature [36, 37, 56, 49] considers the behaviour of the differential operator the models are based on, assuming that the filter length does not tend to zero at the wall, $\overline{\Delta}\big|_\omega = \mathcal{O}(y^0)$. The near-wall order of the models can be obtained from the Taylor series expansion of the velocity and the scalar (density or inverse of density) [10, 46, 12, 37]:

$$U_x|_\omega = \mathcal{O}(y^1), \tag{45}$$

$$U_y|_\omega = \mathcal{O}(y^2), \tag{46}$$

$$U_z|_\omega = \mathcal{O}(y^1), \tag{47}$$

$$\phi|_\omega = \mathcal{O}(y^0). \tag{48}$$

The quadratic behaviour of the wall-normal velocity follows from the mass conservation equation, provided that the density is constant at the walls. This assumption is valid in our case if the time variations of thermodynamical pressure are neglected, since the wall temperatures are imposed. The filter is considered to not alter the asymptotic near-wall behaviour of the variables. This assumption is valid for a top-hat filter as defined in equation (44) with varying filter width. The cubic asymptotic near-wall behaviour of the subgrid term can be recovered, for the "xy" component, from the linear near-wall order of the streamwise velocity and the quadratic near-wall order of the wall-normal velocity [46, 49].

We find that this procedure is not satisfactory for the density-velocity correlation subgrid term. Indeed, it is not able to take into account the fact that $F_{\rho U_j} = \overline{\rho U_j} - \overline{\rho}\,\overline{U}_j$ cannot have a near-wall order below 2 because the filter used, given in equation (44), preserves constant and linear functions. To determine the asymptotic near-wall behaviour of the subgrid terms, we carry out a Taylor series expansion of the filter, leading to the gradient model [27]. Next, the near-wall order of the gradient model is expressed considering a filter with a non-zero order at the wall. For a continuous filter whose size in the wall-normal direction (y) tends to zero at the wall, it is natural to consider

$$\overline{\Delta}_x\big|_\omega = \mathcal{O}(y^0), \tag{49}$$

Subgrid-scale model	With $\overline{\Delta}_y\big\vert_\omega = \mathcal{O}(y^0)$	With $\overline{\Delta}_y\big\vert_\omega = \mathcal{O}(y^1)$
Smagorinsky model [50]	$\mathcal{O}(y^0)$	$\mathcal{O}(y^2)$
WALE model [36]	$\mathcal{O}(y^3)$	$\mathcal{O}(y^{11/3})$
Vreman model [58]	$\mathcal{O}(y^1)$	$\mathcal{O}(y^{3/2})$
Sigma model [37]	$\mathcal{O}(y^3)$	$\mathcal{O}(y^{11/3})$
AMD model [44]	$\mathcal{O}(y^1)$	$\mathcal{O}(y^3)$
Scalar AMD model [2]	$\mathcal{O}(y^0)$	$\mathcal{O}(y^3)$
VSS model [45]	$\mathcal{O}(y^3)$	$\mathcal{O}(y^{11/3})$
Kobayashi model [26]	$\mathcal{O}(y^3)$	$\mathcal{O}(y^{11/3})$
Anisotropic Smagorinsky model	$\mathcal{O}(y^0)$	$\mathcal{O}(y^2)$
MMG model	$\mathcal{O}(y^0)$	$\mathcal{O}(y^2)$
Scalar MMG model	$\mathcal{O}(y^0)$	$\mathcal{O}(y^2)$

Table 1 – Asymptotic near-wall behaviour of the models, for a constant and linear near-wall behaviour of the filter width. The expected order is $\mathcal{O}(y^3)$ for the subgrid term associated with momentum convection and the density-velocity correlation subgrid term.

$$\overline{\Delta}_y\big\vert_\omega = \mathcal{O}(y^1), \tag{50}$$
$$\overline{\Delta}_z\big\vert_\omega = \mathcal{O}(y^0). \tag{51}$$

It follows

$$\overline{\Delta}\big\vert_\omega = \mathcal{O}(y^{1/3}). \tag{52}$$

Note also that the near-wall order of the streamwise and spanwise derivatives of the scalar is at least $\mathcal{O}(y^1)$ under the hypothesis of constant density at the walls. With these assumptions, the expected asymptotic near-wall behaviour of the eddy-diffusivity for models of the density-velocity correlation subgrid term is also cubic with respect to the distance to the wall, $\kappa_e^{\mathrm{mod}}(\boldsymbol{g}, \boldsymbol{d}, \overline{\boldsymbol{\Delta}})\big\vert_\omega = \mathcal{O}(y^3)$. This ensures that the order of the subgrid squared scalar dissipation corresponds to that of the exact subgrid term. For the subgrid term associated with momentum convection, the results are consistent with the literature since it leads to the same near-wall order for each component as the Taylor series expansion of the velocity tensor product.

The asymptotic near-wall behaviour of the investigated subgrid-scale models is given in table 1 for a filter width of order $\mathcal{O}(y^0)$ at the wall and a filter which obeys equations (49–51). With $\overline{\Delta}_y\big\vert_\omega = \mathcal{O}(y^0)$, the WALE, Sigma, VSS and Kobayashi models have the proper asymptotic near-wall behaviour. With $\overline{\Delta}_y\big\vert_\omega = \mathcal{O}(y^1)$, the AMD and scalar AMD models have the proper asymptotic near-wall behaviour.

6 Results and discussion

The performance of the subgrid-scale models is assessed from the comparison of the models and the subgrid terms computed from the DNS data. It is customary [see e.g. 14, 60, 7, 34, 42, 1, 32, 23, 25] to compare the model to the exact subgrid terms using a linear regression analysis. The correlation coefficient is an index scaled to between -1 and 1 which measures the linear correlation between two variables, that is the closeness of the relationship between the two variables with a linear relationship. A value of -1 indicates a perfect negative linear relationship, 0 no linear relationship and 1 a perfect positive linear

relationship. Let us note b a model for the subgrid term of exact value a. The correlation coefficient between a and b is defined by,

$$\mathrm{Corr}(a,b) = \frac{\langle ab\rangle - \langle a\rangle \langle b\rangle}{\sqrt{(\langle a^2\rangle - \langle a\rangle^2)(\langle b^2\rangle - \langle b\rangle^2)}}, \tag{53}$$

where the angle brackets $\langle \cdot \rangle$ denote an ensemble averaging. The regression coefficient gives the slope of the linear relationship,

$$\mathrm{Regr}(a,b) = \frac{\langle ab\rangle - \langle a\rangle \langle b\rangle}{\langle a^2\rangle - \langle a\rangle^2}. \tag{54}$$

The concordance correlation coefficient [30] is a correlation-like index scaled to between -1 and 1 which measure the agreement between two variables, that is the closeness of the relationship between the two variables with identity,

$$\mathrm{Conc}(a,b) = \frac{\langle ab\rangle - \langle a\rangle \langle b\rangle}{\langle a^2\rangle - \langle a\rangle^2 + \langle b^2\rangle - \langle b\rangle^2 + (\langle a\rangle - \langle b\rangle)^2}. \tag{55}$$

The correlation coefficient between the model and the exact subgrid term may be interpreted as the ability of the model to capture the correct flow structure and the regression coefficient of the correct magnitude level. The concordance correlation coefficient combines the two types of information. The optimal value of the correlation coefficient, the regression coefficient and the concordance correlation coefficient is 1. However, only a concordance correlation coefficient of 1 implies that the model and the exact subgrid term are identical.

Given the homogeneity of the flow in the streamwise and spanwise directions, the analysis is carried out as a function of the wall-normal coordinate. The ensemble averaging $\langle \cdot \rangle$ is computed as an average over time and the two homogeneous directions and the linear relationship assessed for each value of y. Notice that the addition for any value of y of a constant scaling factor to the model does not modify the correlation coefficient, multiply the regression coefficient by the constant and has a non-trivial effect on the concordance correlation coefficient.

We first present some general results regarding the performance of the models. Then, the subgrid-scale models are assessed for the subgrid term associated with momentum convection and the density-velocity correlation subgrid term.

6.1 General results

The subgrid-scale modelling in the Velocity and Favre formulations are compared from the study of the subgrid terms and the models with the classical filter and with the Favre filter. The results show no differences between the classical and Favre filter with regard to the performance of the models. For instance, the correlation coefficient between the Smagorinsky model and the exact momentum convection subgrid term with the classical filter and with the Favre filter are very similar (figure 2). The a priori study of the subgrid-scale models thus does not let us select between the Velocity and Favre formulations of the filtered low Mach number equations. Thereafter, the subgrid-scale models are assessed in the Velocity formulation, using the classical filter, but the results also apply to the Favre formulation.

The temperature gradient generates an asymmetry between the hot and cold sides with regard to the performance of the models. This is highlighted in figure 3 by comparing in

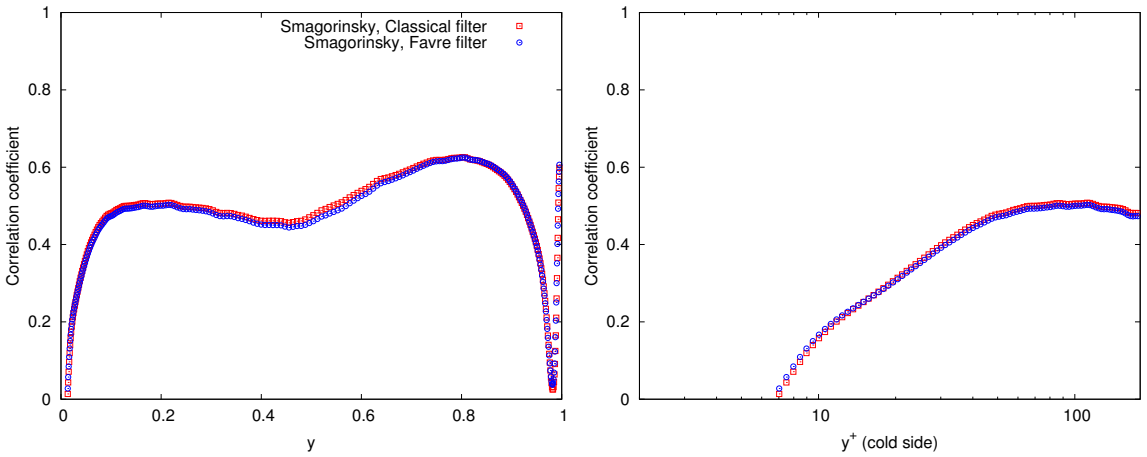

Figure 2 – Correlation coefficient between the exact momentum convection subgrid term and the Smagorinsky model for the term that appears in the streamwise velocity transport equation (6) in the Velocity formulation, $\mathrm{Corr}(\partial_j F_{U_j U_x}, \partial_j \tau_{xj}^{\mathrm{Smag.}}(\overline{\boldsymbol{U}}, \overline{\boldsymbol{\Delta}}))$, and in the streamwise momentum conservation equation (10) in the Favre formulation, $\mathrm{Corr}(\partial_j \bar{\rho} G_{U_j U_x}, \partial_j \bar{\rho} \tau_{ij}^{\mathrm{Smag.}}(\widetilde{\boldsymbol{U}}, \overline{\boldsymbol{\Delta}}))$.

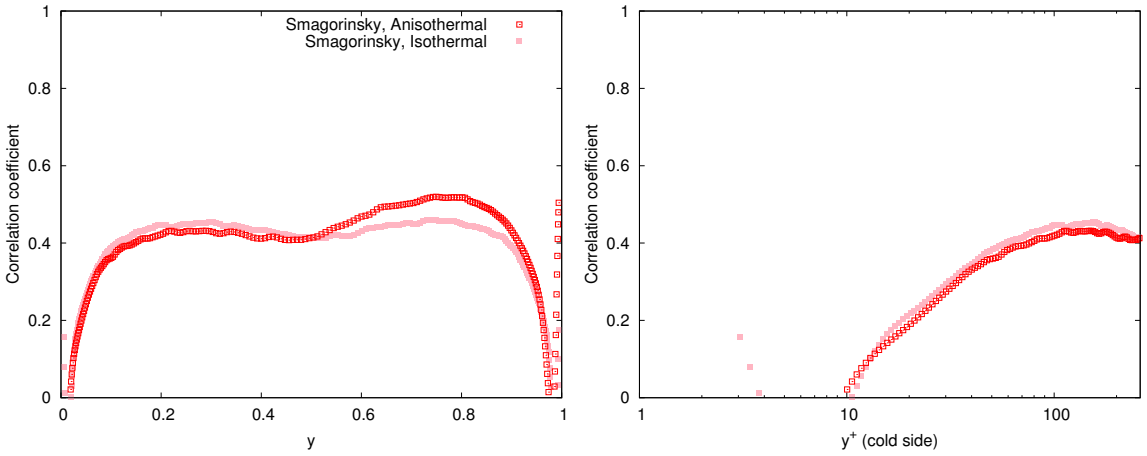

Figure 3 – Correlation coefficient between the divergence of the streamwise-related part of the exact momentum convection subgrid term and the Smagorinsky model, $\mathrm{Corr}(\partial_j F_{U_j U_x}, \partial_j \tau_{xj}^{\mathrm{Smag.}}(\overline{\boldsymbol{U}}, \overline{\boldsymbol{\Delta}}))$, in the isothermal and anisothermal configurations.

the case of the Smagorinsky model the results with an isothermal simulation performed with the same mesh, numerical settings, friction Reynolds number and filtering. The correlation coefficient is larger at the hot side than in the isothermal configuration, and lower at the cold side. The asymmetry may be attributed to an asymmetry of filtering resolution compared to the turbulence intensity. Indeed, due to the variations of the fluid properties with temperature, the local friction Reynolds number varies across the channel, from 105 at the hot wall to 261 at the cold wall, leading to a lower turbulence intensity level at the hot side than in the isothermal configuration, and higher at the cold side.

6.2 Subgrid term associated with momentum convection

The models for the subgrid term associated with momentum convection are assessed as it appears in the streamwise velocity transport equation in figure 4, in the spanwise velocity transport equation in figure 5, and in the wall-normal velocity transport equation in figure 6. The figure 7 addresses the subgrid kinetic energy dissipation $\overline{\rho} F_{U_j U_i} S_{ij}$, an important part of the contribution of the subgrid term to the kinetic energy exchanges. In each case, the profiles of the correlation coefficient, the regression coefficient and the concordance correlation coefficient are given as a function of the wall-normal coordinate y, scaled by the height of the channel, and in the classical wall scaling

$$y^+ = Re_\tau \frac{y}{h} = \frac{y U_\tau}{\nu_\omega}. \tag{56}$$

As a basis of comparison, each model is scaled in order to match the correct level of total subgrid kinetic energy dissipation in the volume. This is equivalent to setting the constant of the models to

$$C^{\mathrm{mod}} = \frac{\int_T \int_V \overline{\rho} F_{U_j U_i} S_{ij} \, dx \, dy \, dz \, dt}{\int_T \int_V \overline{\rho} \tau_{ij}^{\mathrm{mod}}(\boldsymbol{U}, \overline{\boldsymbol{\Delta}}) S_{ij} \, dx \, dy \, dz \, dt}, \tag{57}$$

where V denotes the entire domain and T the integration time.

All the investigated subgrid-scale models correlates rather poorly with the exact subgrid term as it occurs in the velocity transport equation (figures 4(a), 5(a), 6(a)). This is consistent with previous findings which showed that the exact subgrid term correlates poorly with the rate of deformation tensor [32, 14, 31], and reflects the limits of the eddy-viscosity assumption. The models are however better-correlated with the exact subgrid term for the subgrid kinetic energy dissipation (figure 7(a)), with correlation coefficients higher than 0.7–0.8 throughout the channel for the best models. Accordingly, the regression coefficient at the centre of the channel appears too low for all models in the three components of the velocity transport equation (figures 4(b), 5(b), 6(b)), but around an adequate level for the subgrid kinetic energy dissipation (figure 7(b)). This discrepancy is related to the intrinsic nature of the models and may not be easily corrected as increasing the magnitude level of the models to a sufficient amplitude in the velocity transport equation would make the models overdissipative in the kinetic energy transport equation.

The AMD model is significantly more well-correlated with the exact subgrid term than the other investigated models (figures 4(a), 5(a), 6(a), 7(a)). The Vreman, Anisotropic Smagorinsky and MMG models also have a high level of correlation throughout the channel. In the streamwise velocity transport equation (figure 4(a)), the WALE model has a very low correlation coefficient (< 0.2) in the bulk of the channel but gives better results at the wall. In the kinetic energy transport equation (figure 7(a)), it is the opposite. To a lesser extent, the Sigma, VSS and Kobayashi models obey to the same pattern.

Near the wall, the correlation of the Smagorinsky model deteriorates and its amplitude increases dramatically because the differential operator it is based on does not vanish in near-wall regions, which conflicts with the near-wall behaviour of the exact subgrid term. The Anisotropic Smagorinsky model is able to improve greatly the near-wall behaviour of the Smagorinsky model, the filter lengths in the Anisotropic Smagorinsky model acting akin to a damping function. The Vreman, Anisotropic Smagorinsky and MMG models vanish at the wall but with a lower order than the exact subgrid term (table 1). Their magnitude compared to the exact subgrid term is increased near the wall. Nevertheless, their regression coefficient is subject to less variations across throughout the channel than

the WALE, Sigma, VSS and Kobayashi models (figures 4(b), 5(b), 6(b), 7(b)), up to the first point of the LES mesh that the filter represents.

The profile of the subgrid kinetic energy dissipation is given in figure 8. Compared to the exact subgrid term, the Smagorinsky, Vreman, Anisotropic Smagorinsky and MMG models are overdissipative in the near-wall region and underdissipative at the centre of the channel, while the WALE, Sigma, VSS and Kobayashi models dissipates more at the centre of the channel and less near the wall. This corresponds to the models theoretically predicted to lead to, respectively, a lower and a higher near-wall order than the exact subgrid term with a filter such that $\overline{\Delta}_y\big|_\omega = \mathcal{O}(y^1)$ (table 1).

The maximum of subgrid kinetic energy dissipation is located at $y^+ = 12$ at the cold side and $y^+ = 10$ at the hot side, in the range of the turbulence kinetic energy production [19]. Its location is mispredicted towards the centre of the channel by the WALE, Sigma, VSS and Kobayashi models and towards the wall by the Vreman, Anisotropic Smagorinsky and MMG models. The AMD model predicts quite accurately the location of the maximum of subgrid kinetic energy dissipation. It is underdissipative at the cold side and slightly overdissipative at the hot side, meaning that the asymmetry between the hot and cold side is not fully captured by the model.

Eddy-viscosity models are by construction purely dissipative. They represent relatively well the exact subgrid term for the negative values of the subgrid kinetic energy dissipation, which corresponds to a kinetic energy transfer from the resolved to subgrid scales, but cannot represent positive values of the subgrid kinetic energy dissipation. This readily appears in the probability density function of the subgrid kinetic energy dissipation, given in figure 9. While this is a desirable characteristic for numerical stability, this is inconsistent with the behaviour of the exact subgrid term which locally transfer the energy from the subgrid to resolved scales. The backscatter region amounts to 21% of the points in the domain.

Overall, the models in better agreement with the exact subgrid term are the AMD model, followed by the Vreman, Anisotropic Smagorinsky and MMG models (figures 4(c), 5(c), 6(c), 7(c)). Note that in the a priori tests, the performance of the AMD model is not significantly undermined by the clipping of negative viscosity or diffusivity.

6.3 Density velocity correlation subgrid term

The models for the density-velocity correlation subgrid term are assessed as it appears in the mass conservation equation in figure 10 and the subgrid squared scalar dissipation $F_{\rho U_j} d_j$ is addressed in figure 11. As a basis of comparison, each model is scaled in order to match the correct level of total subgrid squared scalar dissipation in the volume. This is equivalent to a modification of the subgrid-scale Prandtl or Schmidt number, or to setting the constant of the models to

$$C^{\mathrm{mod}} = \frac{\int_T \int_V F_{\rho U_j} d_j \, dx \, dy \, dz \, dt}{\int_T \int_V \pi_j^{\mathrm{mod}}(\overline{\boldsymbol{U}}, \overline{\rho}, \overline{\boldsymbol{\Delta}}) d_j \, dx \, dy \, dz \, dt}, \tag{58}$$

with $Pr_t = 1$.

The correlation coefficient of the most models with the exact subgrid term as it appears in the mass conservation equation (figure 10(a)) reaches a maximum in the range 0.3–0.6, is lower at the centre of the channel and falls to or below zero near the wall. The WALE model is here an exception as its correlation with the exact subgrid term is very poor in the entire

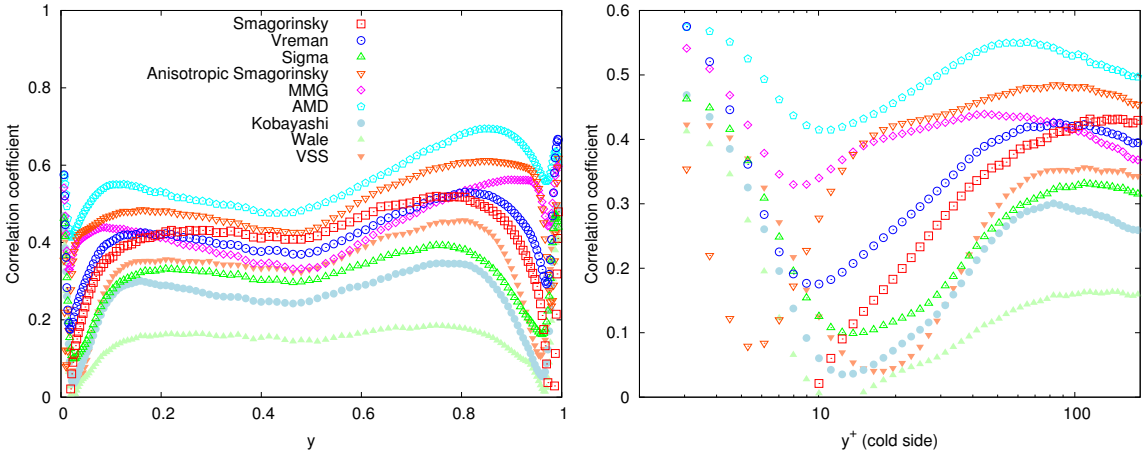

(a) Correlation coefficient.

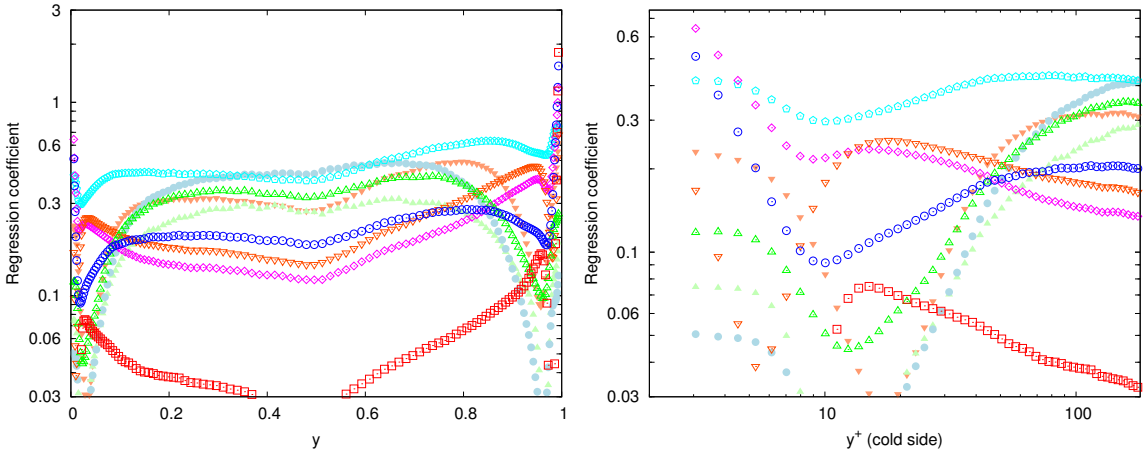

(b) Regression coefficient.

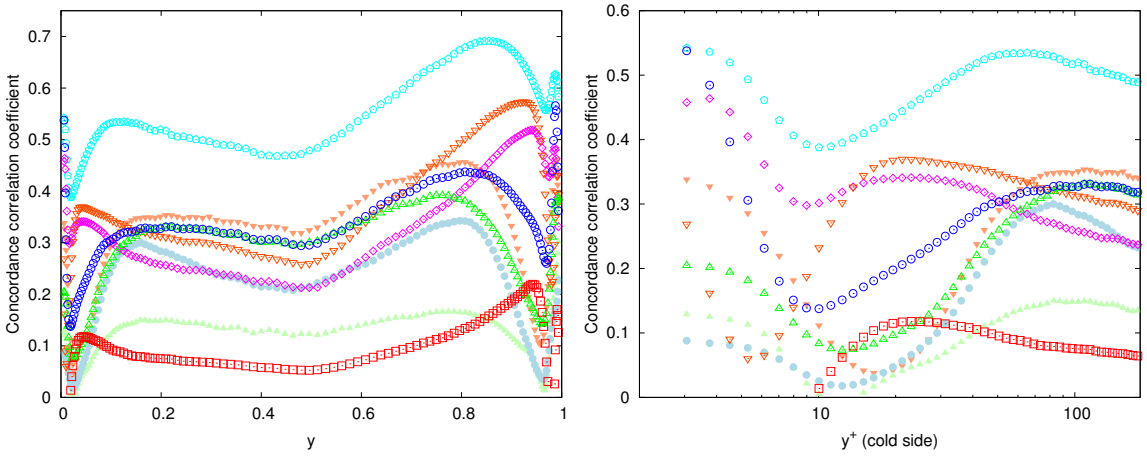

(c) Concordance correlation coefficient.

Figure 4 – Correlation coefficient, regression coefficient, and concordance correlation coefficient between the divergence of the streamwise-related part of the exact momentum convection subgrid term $\partial_j F_{U_j U_x}$ and eddy-viscosity models $\partial_j \tau_{xj}^{\mathrm{mod}}(\overline{\boldsymbol{U}}, \overline{\boldsymbol{\Delta}})$.

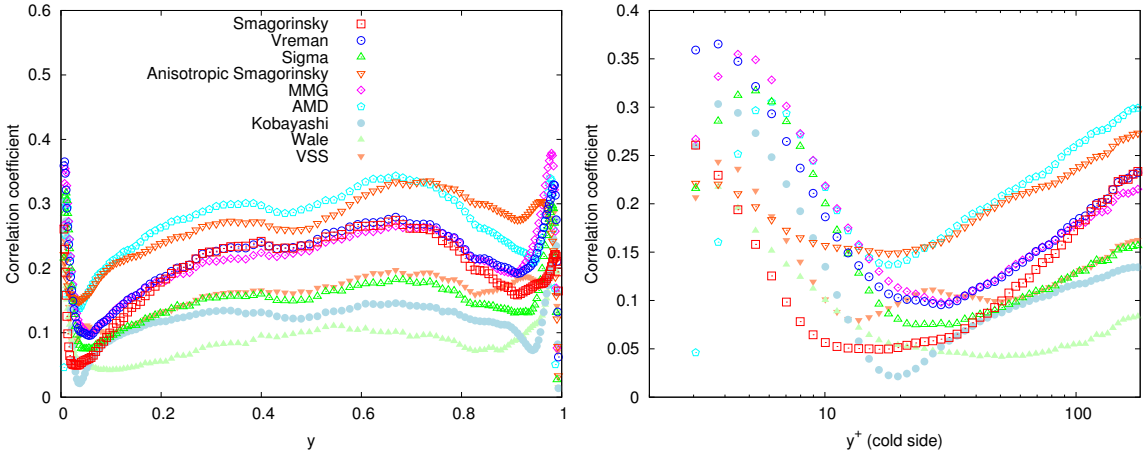

(a) Correlation coefficient.

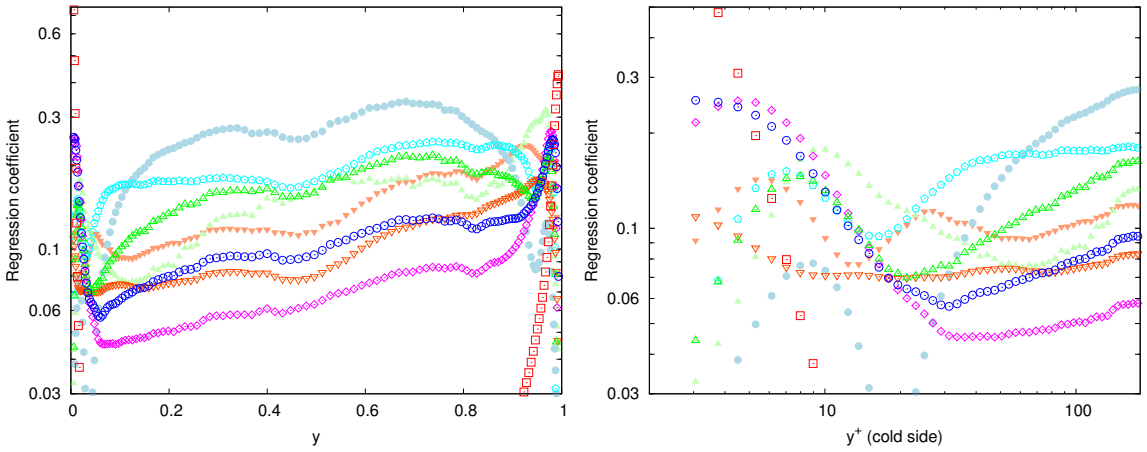

(b) Regression coefficient.

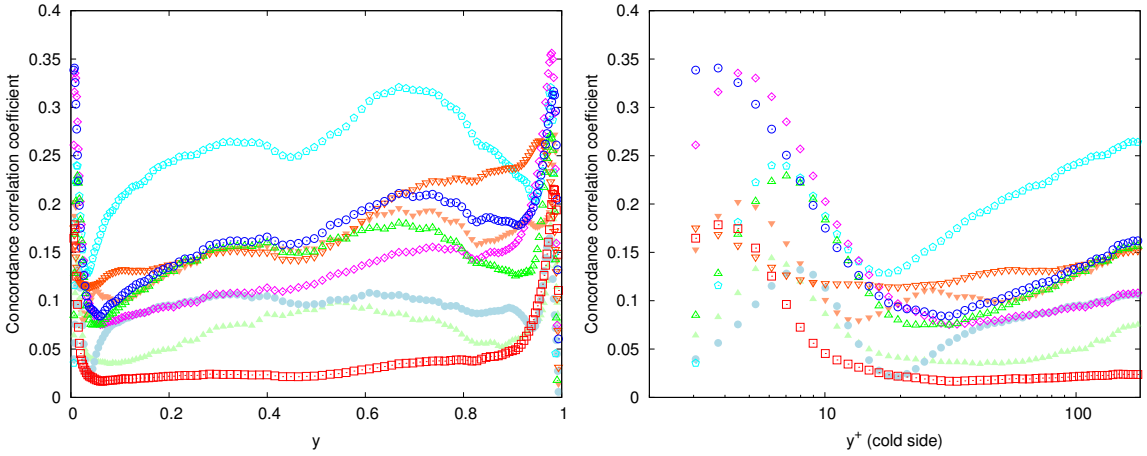

(c) Concordance correlation coefficient.

Figure 5 – Correlation coefficient, regression coefficient, and concordance correlation coefficient between the divergence of the spanwise-related part of the exact momentum convection subgrid term $\partial_j F_{U_j U_z}$ and eddy-viscosity models $\partial_j \tau_{zj}^{\mathrm{mod}}(\overline{\boldsymbol{U}}, \overline{\boldsymbol{\Delta}})$.

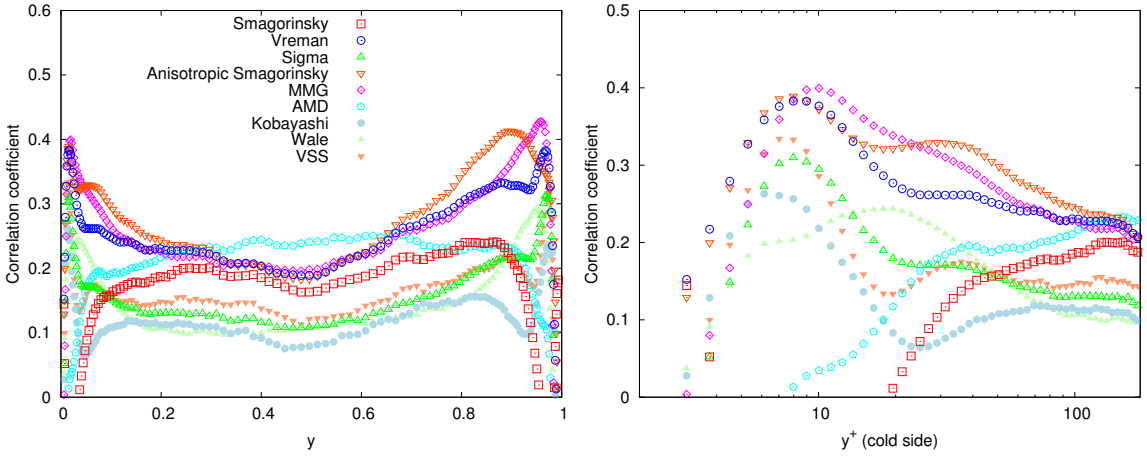

(a) Correlation coefficient.

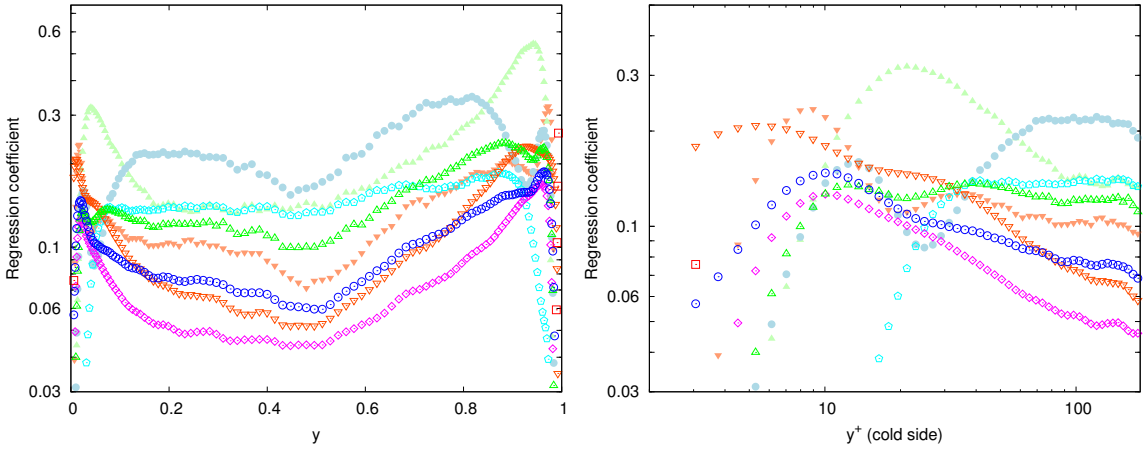

(b) Regression coefficient.

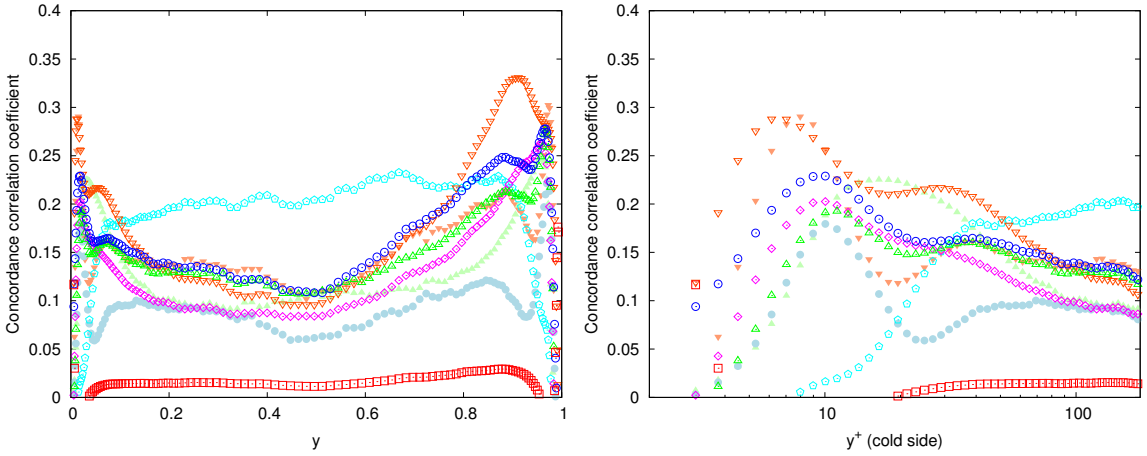

(c) Concordance correlation coefficient.

Figure 6 – Correlation coefficient, regression coefficient, and concordance correlation coefficient between the divergence of the wall-normal-related part of the exact momentum convection subgrid term $\partial_j F_{U_j U_y}$ and eddy-viscosity models $\partial_j \tau_{yj}^{\mathrm{mod}}(\overline{\boldsymbol{U}}, \overline{\boldsymbol{\Delta}})$.

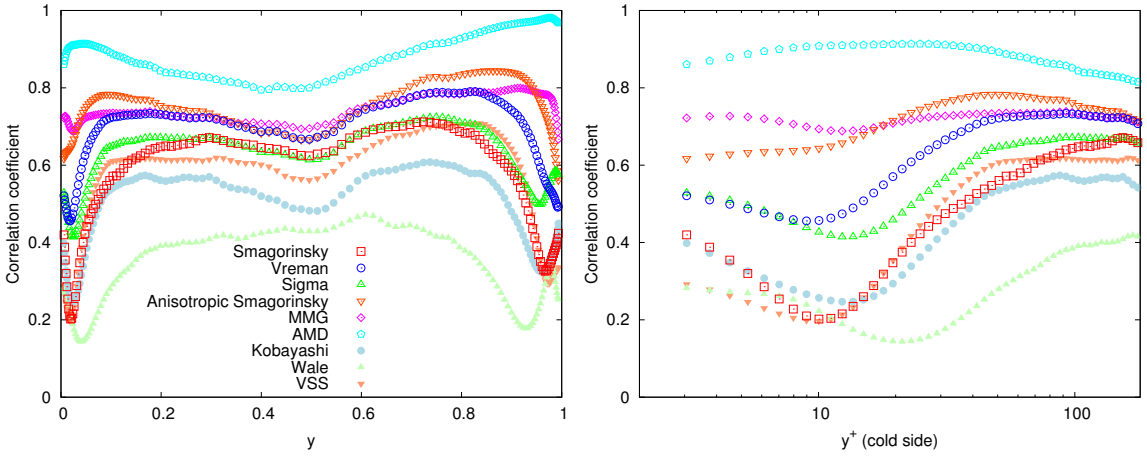

(a) Correlation coefficient.

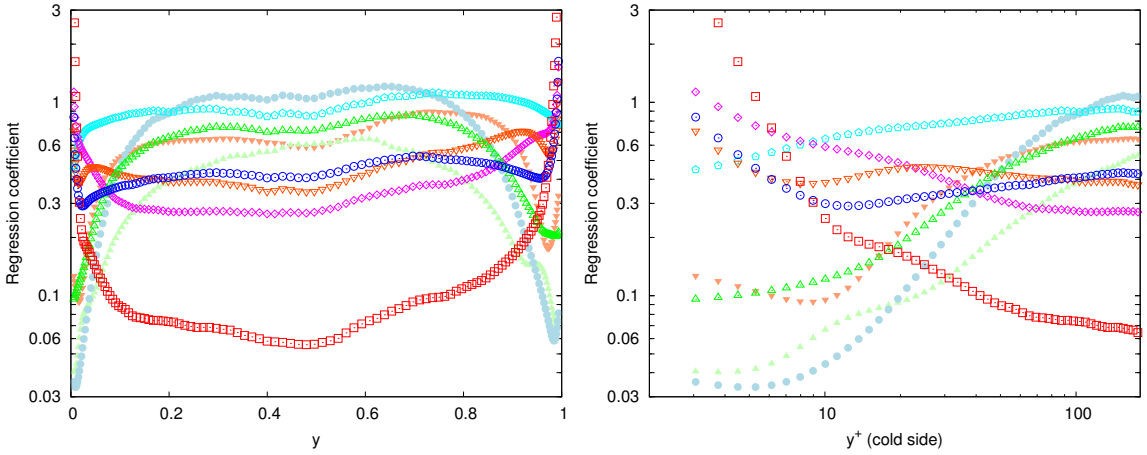

(b) Regression coefficient.

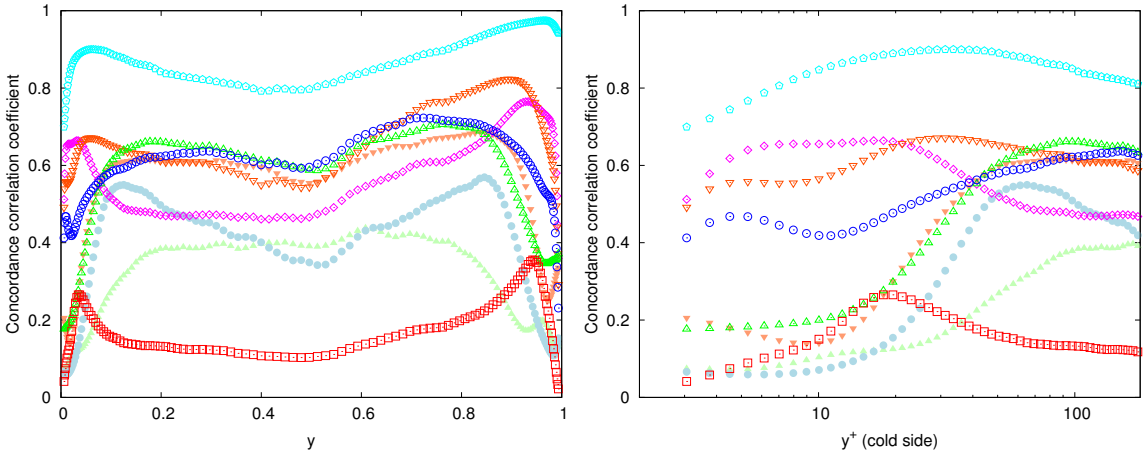

(c) Concordance correlation coefficient.

Figure 7 – Correlation coefficient, regression coefficient, and concordance correlation coefficient between the subgrid kinetic energy dissipation of the exact momentum convection subgrid term $\bar{\rho} F_{U_j U_i} S_{ij}$ and eddy-viscosity models $\bar{\rho} \tau_{ij}^{\mathrm{mod}}(\overline{\boldsymbol{U}}, \overline{\boldsymbol{\Delta}}) S_{ij}$.

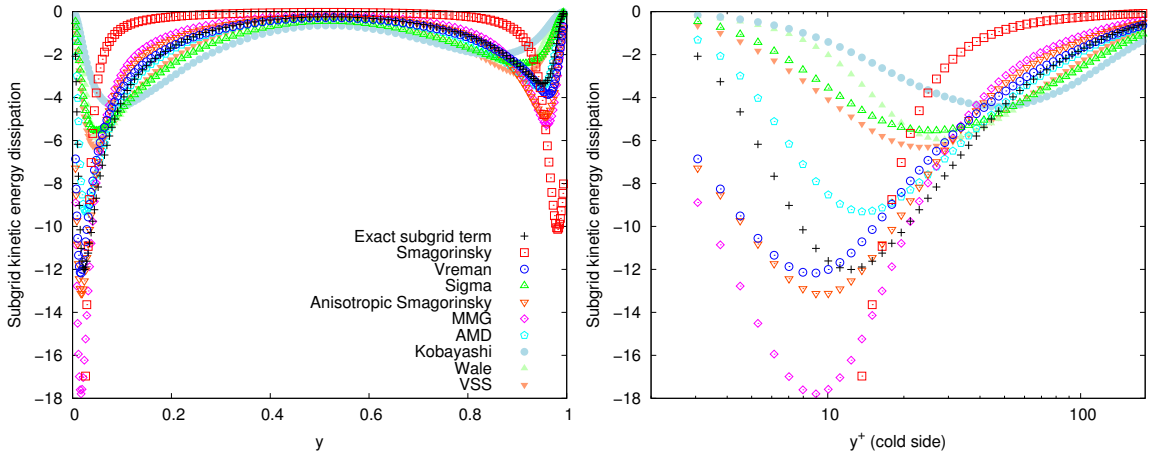

Figure 8 – Profile of the statistical average of the subgrid kinetic energy dissipation of the exact momentum convection subgrid term $\overline{\rho} F_{U_j U_i} S_{ij}$ and eddy-viscosity models $\overline{\rho} \tau_{ij}^{\mathrm{mod}}(\overline{\boldsymbol{U}}, \overline{\boldsymbol{\Delta}}) S_{ij}$.

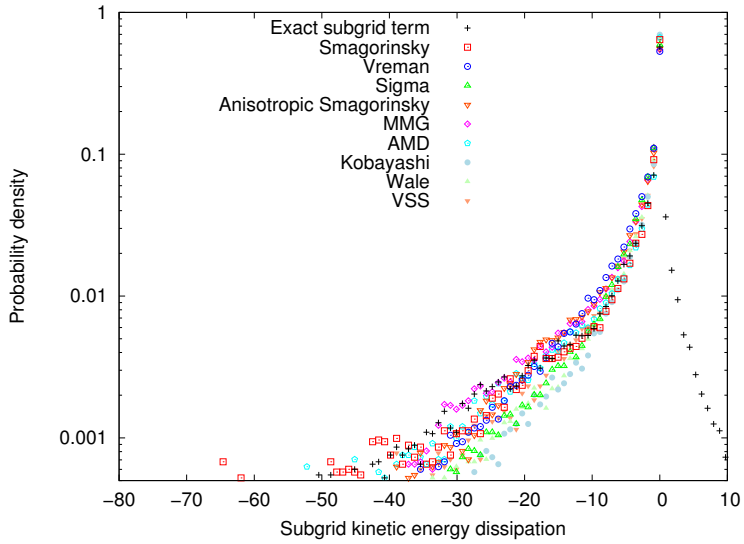

Figure 9 – Probability density function of the subgrid kinetic energy dissipation of the exact momentum convection subgrid term $\overline{\rho} F_{U_j U_i} S_{ij}$ and eddy-viscosity models $\overline{\rho} \tau_{ij}^{\mathrm{mod}}(\overline{\boldsymbol{U}}, \overline{\boldsymbol{\Delta}}) S_{ij}$.

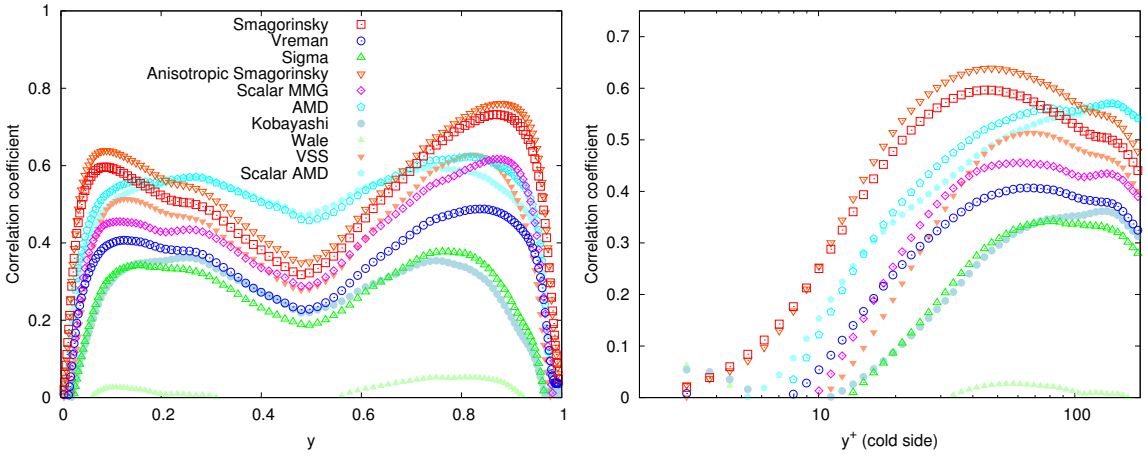

(a) Correlation coefficient.

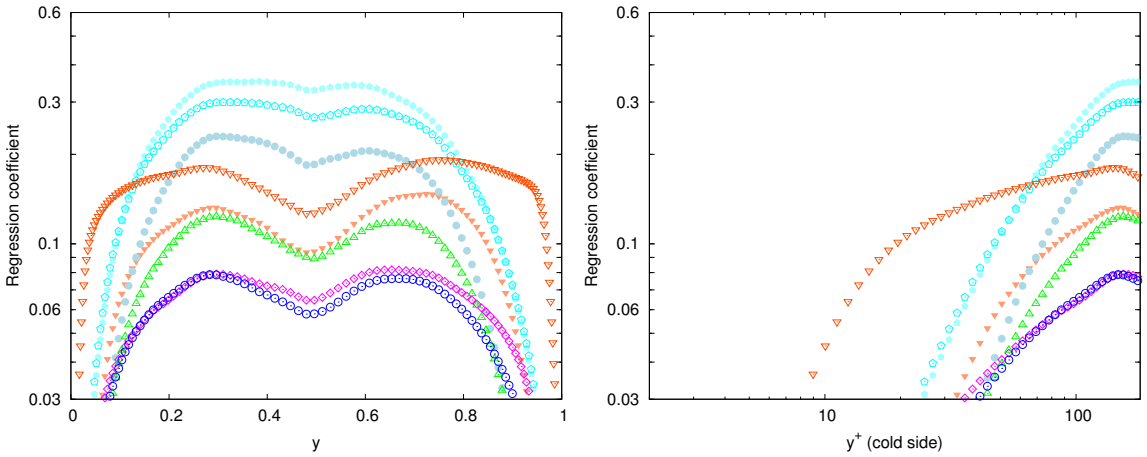

(b) Regression coefficient.

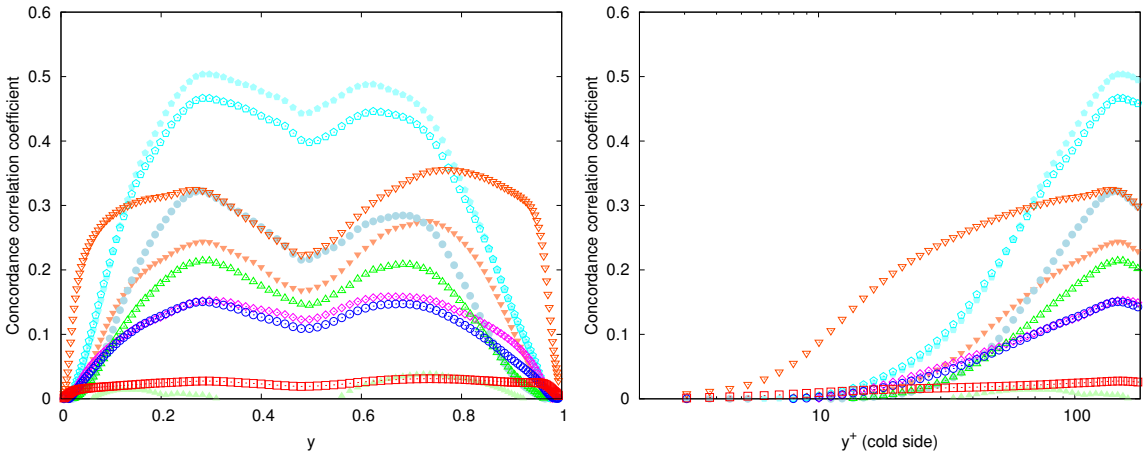

(c) Concordance correlation coefficient.

Figure 10 – Correlation coefficient, regression coefficient, and concordance correlation coefficient between the divergence of the exact density-velocity correlation subgrid term $\partial_j F_{\rho U_j}$ and eddy-diffusivity models $\partial_j \pi_j^{\mathrm{mod}}(\overline{\boldsymbol{U}}, \overline{\rho}, \overline{\boldsymbol{\Delta}})$.

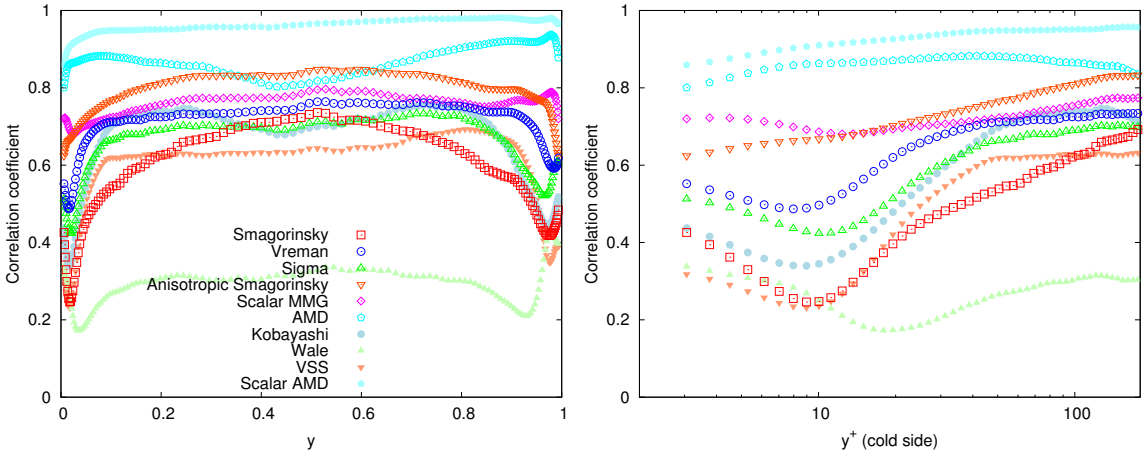

(a) Correlation coefficient.

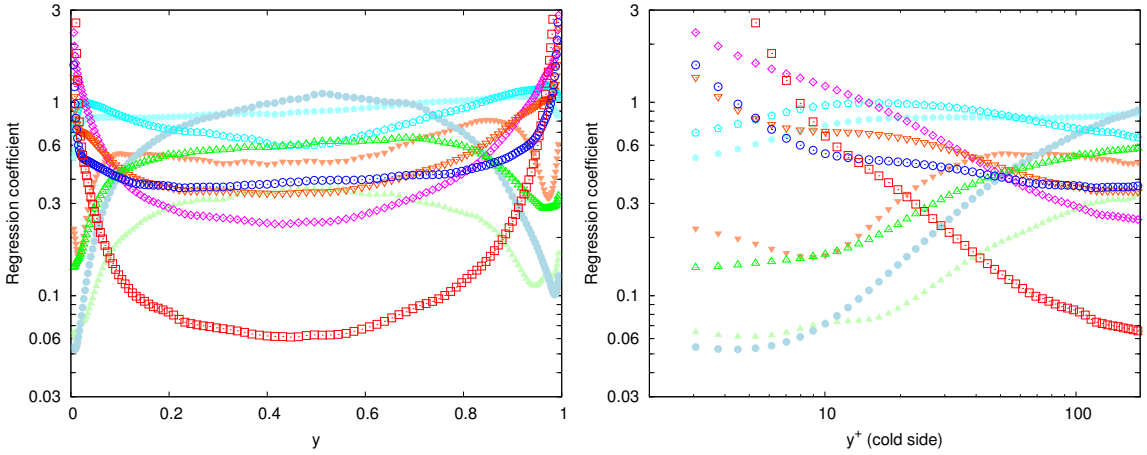

(b) Regression coefficient.

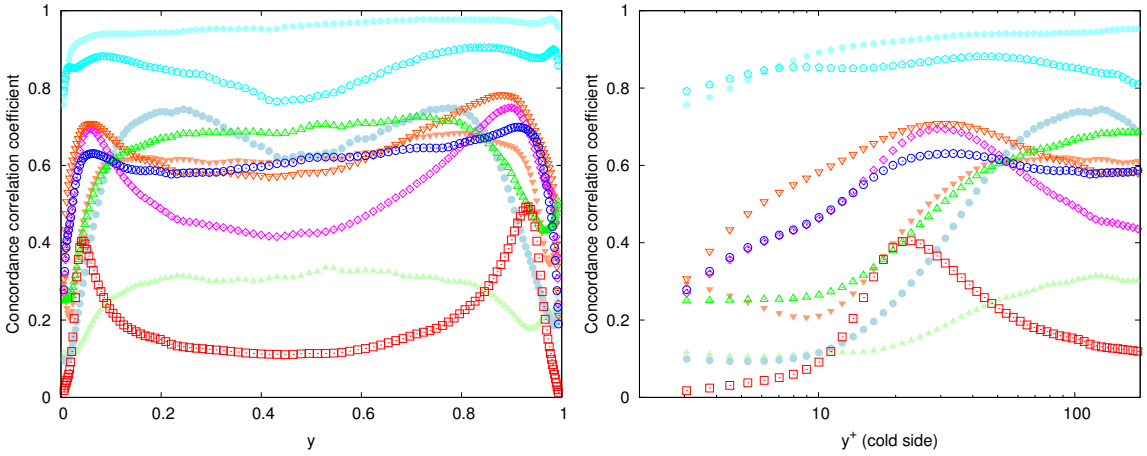

(c) Concordance correlation coefficient.

Figure 11 – Correlation coefficient, regression coefficient, and concordance correlation coefficient between the subgrid squared scalar dissipation of the exact density-velocity correlation subgrid term $F_{\rho U_j} d_j$ and eddy-diffusivity models $\pi_j^{\mathrm{mod}}(\overline{\boldsymbol{U}}, \overline{\rho}, \overline{\boldsymbol{\Delta}}) d_j$.

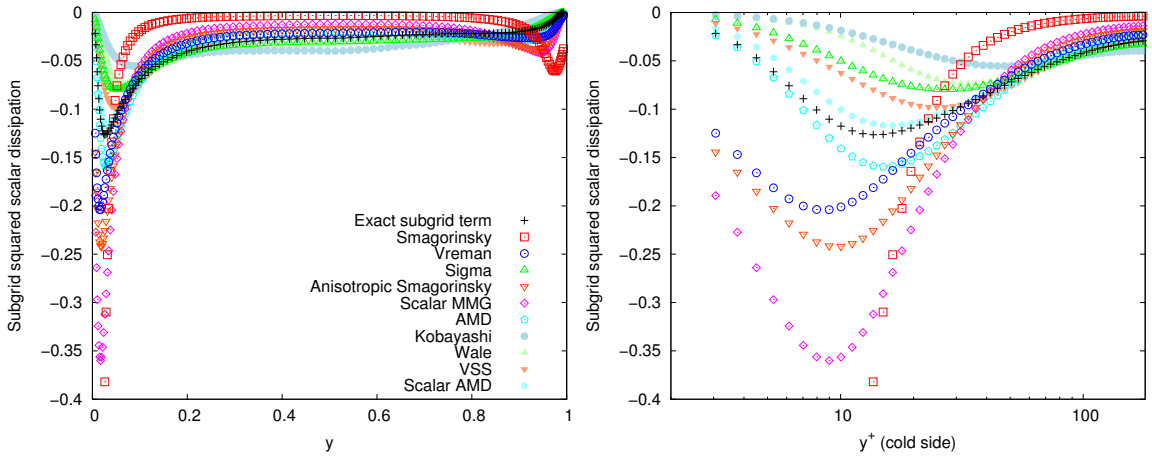

Figure 12 – Profile of the statistical average of the subgrid squared scalar dissipation of the exact density-velocity correlation subgrid term $F_{\rho U_j} d_j$ and eddy-diffusivity models $\pi_j^{\mathrm{mod}}(\overline{\boldsymbol{U}}, \overline{\rho}, \overline{\boldsymbol{\Delta}}) d_j$.

channel. At the centre of the channel, the AMD and scalar AMD models have the largest correlation coefficient. This may indicate their relevance in far-from-wall flows. Within the influence of the wall, the most well-correlated models are the Smagorinsky model and the Anisotropic Smagorinsky model, which is able to slightly improve the correlation of the Smagorinsky model. As the correlation coefficient, the regression coefficient declines from the logarithmic layer to the wall (figure 10(b)), meaning that the investigated subgrid-scale models fall too rapidly to zero at the wall. The drop occurs nearer to the wall with the Anisotropic Smagorinsky model. The Anisotropic Smagorinsky, AMD and scalar AMD models are overall in a better agreement with the exact subgrid term (figure 10(c)).

Similarly to eddy-viscosity models, larger correlation coefficients are found for the subgrid squared scalar dissipation (figure 11(a)). The AMD and scalar AMD models are clearly the models that represent the more accurately the exact subgrid squared scalar dissipation (figure 11(c)), with in the entire channel a correlation coefficient over 0.8 (figure 11(a)) and a regression coefficient in the range 0.5–1 (figure 11(b)). The scalar AMD model provides an improvement compared to the AMD model developed for the momentum convection subgrid term. An increase of the regression coefficient of the Smagorinsky, Vreman, Anisotropic Smagorinsky and MMG models is observed near the wall, while the regression coefficient of the WALE, Sigma, VSS and Kobayashi models models stabilises to a low value (figure 11(b)). The profile of the subgrid squared scalar dissipation (figure 12) shows that the Smagorinsky, Vreman, Anisotropic Smagorinsky and MMG models are overdissipative in the near-wall region and underdissipative at the centre of the channel compared to the exact subgrid term, and conversely for the WALE, Sigma, VSS and Kobayashi models. These results are identical to the results obtained for the subgrid kinetic energy dissipation. The profile of the ratio of the subgrid kinetic energy dissipation and the subgrid squared scalar dissipation (figure 13) shows that they have the same near-wall order. The results are thus consistent with our theoretical analysis of the asymptotic near-wall behaviour of the subgrid terms.

The eddy-diffusivity assumption is as appropriate as the eddy-viscosity assumption, in the sense the same amount of backscatter is observed for the subgrid squared scalar dissipation than for the subgrid kinetic energy dissipation, as can be seen in the probability density function of the subgrid squared scalar dissipation (figure 14). However, it may be

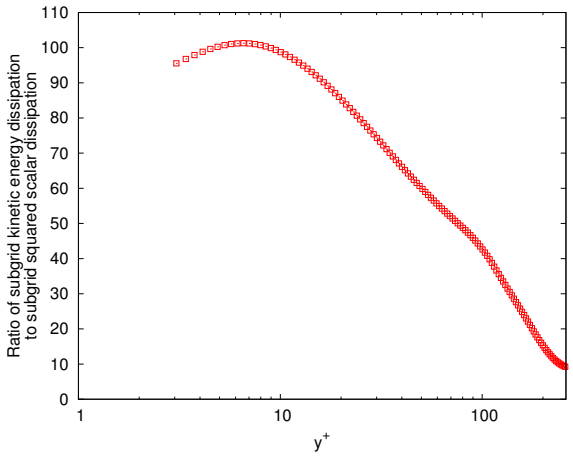

Figure 13 – Profile of the ratio of the statistical average of the subgrid kinetic energy dissipation and the subgrid squared scalar dissipation, $[\overline{\rho} F_{U_j U_i} S_{ij}]/[F_{\rho U_j} d_j]$.

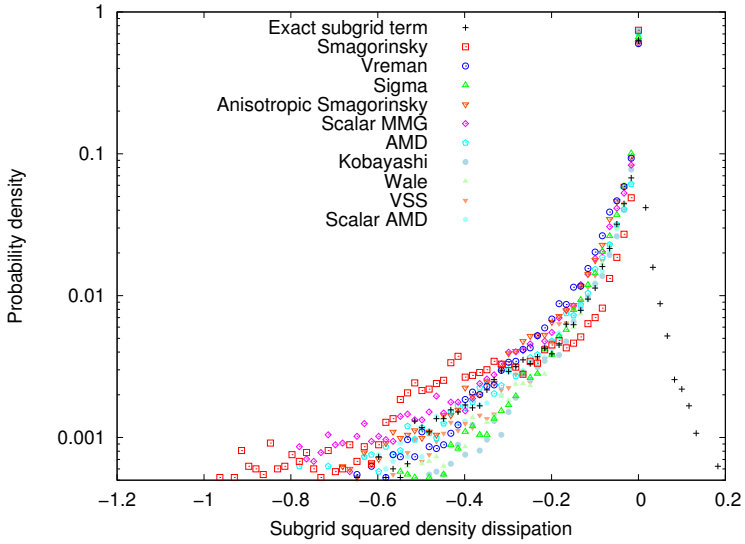

Figure 14 – Probability density function of the subgrid squared scalar dissipation of the exact density-velocity correlation subgrid term $F_{\rho U_j} d_j$ and eddy-diffusivity models $\pi_j^{\mathrm{mod}}(\overline{\boldsymbol{U}}, \overline{\rho}, \overline{\boldsymbol{\Delta}}) d_j$.

argued that the behaviour of the subgrid squared scalar dissipation is less critical than the subgrid kinetic energy dissipation for the numerical stability of a numerical simulation, suggesting that more emphasis should be placed on the relevance of the model as it appears in the mass conservation equation.

Overall, the models in better agreement with the exact subgrid term are the AMD and scalar AMD models, followed by the Vreman, Anisotropic Smagorinsky and MMG models (figures 10(c), 11(c)). They are the same models than for the subgrid term associated with momentum convection.

7 Conclusion

The filtering of the low Mach number equations with the unweighted classical filter or the density-weighted Favre filter leads to specific subgrid terms. The two most significant subgrid terms are the subgrid terms associated with the momentum convection and the density-velocity correlation. They are compared to subgrid-scale models using the flow field from direct numerical simulations of a strongly anisothermal turbulent channel flow. Classical and Favre filter are found to have no influence on the performance of the models. Eddy-viscosity and eddy-diffusivity models are shown to be in better agreement with the subgrid kinetic energy dissipation and the subgrid squared scalar dissipation respectively than with the contribution of the subgrid terms in the filtered low Mach number equations. However, eddy-viscosity and eddy-diffusivity models are not able to account for backscatter, present in a fifth of the points in the domain. The AMD and scalar AMD models perform better than the other investigated models with regard to the correlation coefficient, regression coefficient and concordance correlation coefficient with the exact subgrid term. This may be attributed to the strong link between the AMD and scalar AMD models and the gradient model. The AMD and scalar AMD inherit from the gradient model a similarity with the exact subgrid term but, unlike the gradient model, are purely dissipative and should not lead to numerical stability issues.

Acknowledgment

The authors gratefully acknowledge the CEA for the development of the TRUST platform. This work was granted access to the HPC resources of CINES under the allocations 2017-A0022A05099 and 2018-A0042A05099 made by GENCI.

References

[1] A. Abba, A. C. Cercignani, and L. Valdettaro. Analysis of subgrid scale models. *Comput. Math. Appl.*, 46(4):521–535, 2003.

[2] M. Abkar, H. J. Bae, and P. Moin. Minimum-dissipation scalar transport model for large-eddy simulation of turbulent flows. *Physical Review Fluids*, 1(4):041701, 2016.

[3] F. Aulery, D. Dupuy, A. Toutant, F. Bataille, and Y. Zhou. Spectral analysis of turbulence in anisothermal channel flows. *Computers & Fluids*, 151:115–131, 2017.

[4] J. Bardina, J. Ferziger, and W. C. Reynolds. Improved subgrid-scale models for large-eddy simulation. In *13th Fluid and PlasmaDynamics Conference*, page 1357, 1980.

[5] L. C. Berselli, T. Iliescu, and W. J. Layton. *Mathematics of large eddy simulation of turbulent flows*. Springer Science & Business Media, 2005.

[6] G. Borghesi and J. Bellan. A priori and a posteriori investigations for developing large eddy simulations of multi-species turbulent mixing under high-pressure conditions. *Physics of Fluids*, 27(3):035117, 2015.

[7] V. Borue and S. A. Orszag. Local energy flux and subgrid-scale statistics in three-dimensional turbulence. *Journal of Fluid Mechanics*, 366:1–31, 1998.

[8] M. Breuer and F. Hoppe. Influence of a cost–efficient langevin subgrid-scale model on the dispersed phase of large–eddy simulations of turbulent bubble–laden and particle–laden flows. *International Journal of Multiphase Flow*, 89:23–44, 2017.

[9] C. Calvin, O. Cueto, and P. Emonot. An object-oriented approach to the design of fluid mechanics software. *ESAIM: Mathematical Modelling and Numerical Analysis*, 36(05):907–921, 2002.

[10] D. R. Chapman and G. D. Kuhn. The limiting behaviour of turbulence near a wall. *Journal of Fluid Mechanics*, 170:265–292, 1986.

[11] J. Chen and G. Jin. Large-eddy simulation of turbulent preferential concentration and collision of bidisperse heavy particles in isotropic turbulence. *Powder Technology*, 314:281–290, 2017.

[12] M. S. Chong, J. P. Monty, C. Chin, and I. Marusic. The topology of skin friction and surface vorticity fields in wall-bounded flows. *Journal of Turbulence*, (13):N6, 2012.

[13] S. G. Chumakov and C. J. Rutland. Dynamic structure subgrid-scale models for large eddy simulation. *International Journal for Numerical Methods in Fluids*, 47(8-9):911–923, 2005.

[14] R. A. Clark, J. H. Ferziger, and W. C. Reynolds. Evaluation of subgrid-scale models using an accurately simulated turbulent flow. *Journal of Fluid Mechanics*, 91(1):1–16, 1979.

[15] J. W. Deardorff. A numerical study of three-dimensional turbulent channel flow at large reynolds numbers. *Journal of Fluid Mechanics*, 41(2):453–480, 1970.

[16] D. Dupuy, A. Toutant, and F. Bataille. Study of the sub-grid terms of the large-eddy simulation of a low Mach strongly anisothermal channel flow. In *Eurotherm Seminar 106, Paris, France*, 2016.

[17] D. Dupuy, A. Toutant, and F. Bataille. étude de l'équation d'énergie pour le développement de modèles sous-mailles adaptés aux écoulements fortement anisothermes. In *Congrès SFT, Marseille, France*, 2017.

[18] D. Dupuy, A. Toutant, and F. Bataille. Study of the large-eddy simulation subgrid terms of a low mach number anisothermal channel flow. *International Journal of Thermal Sciences*, 135:221–234, 2018.

[19] D. Dupuy, A. Toutant, and F. Bataille. Turbulence kinetic energy exchanges in flows with highly variable fluid properties. *Journal of Fluid Mechanics*, 834:5–54, 2018.

[20] A. Favre. The equations of compressible turbulent gases. Technical Report AD0622097, DTIC Document, 1965.

[21] K. Fröhlich, L. Schneiders, M. Meinke, and W. Schröder. Validation of lagrangian two-way coupled point-particle models in large-eddy simulations. *Flow, Turbulence and Combustion*, pages 1–25, 2018.

[22] M. Germano, U. Piomelli, P. Moin, and W. H. Cabot. A dynamic subgrid-scale eddy viscosity model. *Physics of Fluids A: Fluid Dynamics*, 3(7):1760–1765, 1991.

[23] N. S. Ghaisas and S. H. Frankel. A priori evaluation of large eddy simulation subgrid-scale scalar flux models in isotropic passive-scalar and anisotropic buoyancy-driven homogeneous turbulence. *J. Turbulence*, 15(2):88–121, 2014.

[24] N. S. Ghaisas and S. H. Frankel. Dynamic gradient models for the sub-grid scale stress tensor and scalar flux vector in large eddy simulation. *Journal of Turbulence*, 17(1):30–50, 2016.

[25] S. Ketterl and M. Klein. A-priori assessment of subgrid scale models for large-eddy simulation of multiphase primary breakup. *Computers & Fluids*, 165:64–77, 2018.

[26] H. Kobayashi. The subgrid-scale models based on coherent structures for rotating homogeneous turbulence and turbulent channel flow. *Physics of Fluids*, 17(4):045104, 2005.

[27] A. Leonard. Energy cascade in large eddy simulations of turbulent fluid flows. *Advances in Geophysics*, 18A:237–248, 1974.

[28] C. Li. *A-priori analysis of LES subgrid scale models applied to wall turbulence with pressure gradients*. PhD thesis, Ecole Centrale de Lille, 2013.

[29] D. K. Lilly. A proposed modification of the germano subgrid-scale closure method. *Physics of Fluids A: Fluid Dynamics*, 4(3):633–635, 1992.

[30] L. I.-K. Lin. A concordance correlation coefficient to evaluate reproducibility. *Biometrics*, pages 255–268, 1989.

[31] S. Liu, C. Meneveau, and J. Katz. On the properties of similarity subgrid-scale models as deduced from measurements in a turbulent jet. *Journal of Fluid Mechanics*, 275:83–119, 1994.

[32] H. Lu, C. J. Rutland, and L. M. Smith. A priori tests of one-equation LES modeling of rotating turbulence. *J. Turbulence*, (8):N37, 2007.

[33] C. Marchioli. Large-eddy simulation of turbulent dispersed flows: a review of modelling approaches. *Acta Mechanica*, 228(3):741–771, 2017.

[34] M. Pino Martín, U. Piomelli, and G. V. Candler. Subgrid-scale models for compressible large-eddy simulations. *Theoretical and Computational Fluid Dynamics*, 13(5):361–376, 2000.

[35] F. Nicoud. Conservative high-order finite-difference schemes for low-Mach number flows. *J. Comput. Phys.*, 158(1):71–97, 2000.

[36] F. Nicoud and F. Ducros. Subgrid-scale stress modelling based on the square of the velocity gradient tensor. *Flow, Turbulence and Combustion*, 62(3):183–200, 1999. ISSN 1386-6184.

[37] F. Nicoud, H. Baya Toda, O. Cabrit, S. Bose, and J. Lee. Using singular values to build a subgrid-scale model for large eddy simulations. *Physics of Fluids*, 23(8):085106, 2011.

[38] S. Paolucci. On the filtering of sound from the Navier–Stokes equations. Technical Report SAND82-8257, Sandia National Labs., Livermore, CA (USA), 1982.

[39] G. I. Park, M. Bassenne, J. Urzay, and P. Moin. A simple dynamic subgrid-scale model for les of particle-laden turbulence. *Physical Review Fluids*, 2(4):044301, 2017.

[40] N. Park, S. Lee, J. Lee, and H. Choi. A dynamic subgrid-scale eddy viscosity model with a global model coefficient. *Physics of Fluids*, 18(12):125109, 2006.

[41] U. Piomelli, P. Moin, and J. H. Ferziger. Model consistency in large eddy simulation of turbulent channel flows. *Physics of Fluids*, 31(7):1884–1891, 1988.

[42] C. D. Pruett and N. A. Adams. A priori analyses of three subgrid-scale models for one-parameter families of filters. *Physics of Fluids*, 12(5):1133–1142, 2000.

[43] B. Rosa and J. Pozorski. Impact of subgrid fluid turbulence on inertial particles subject to gravity. *Journal of Turbulence*, 18(7):634–652, 2017.

[44] W. Rozema, H.J. Bae, P. Moin, and R. Verstappen. Minimum-dissipation models for large-eddy simulation. *Physics of Fluids*, 27(8):085107, 2015.

[45] S. Ryu and G. Iaccarino. A subgrid-scale eddy-viscosity model based on the volumetric strain-stretching. *Physics of Fluids*, 26(6):065107, 2014.

[46] P. Sagaut. *Large eddy simulation for incompressible flows: an introduction*. Springer Science & Business Media, 2006.

[47] F. Sarghini, U. Piomelli, and E. Balaras. Scale-similar models for large-eddy simulations. *Physics of Fluids*, 11(6):1596–1607, 1999.

[48] S. Serra, A. Toutant, F. Bataille, and Y. Zhou. High-temperature gradient effect on a turbulent channel flow using thermal large-eddy simulation in physical and spectral spaces. *J. Turbulence*, 13:N49, 2012.

[49] M. H. Silvis, R. A. Remmerswaal, and R. Verstappen. Physical consistency of subgrid-scale models for large-eddy simulation of incompressible turbulent flows. *Physics of Fluids*, 29(1): 015105, 2017.

[50] J. Smagorinsky. General circulation experiments with the primitive equations: I. the basic experiment. *Monthly weather review*, 91(3):99–164, 1963.

[51] W. Sutherland. The viscosity of gases and molecular force. *The London, Edinburgh, and Dublin Philosophical Magazine and Journal of Science*, 36(223):507–531, 1893.

[52] A. Toutant and F. Bataille. Turbulence statistics in a fully developed channel flow submitted to a high temperature gradient. *International Journal of Thermal Sciences*, 74:104–118, 2013.

[53] A. Toutant, E. Labourasse, O. Lebaigue, and O. Simonin. DNS of the interaction between a deformable buoyant bubble and a spatially decaying turbulence: a priori tests for LES two-phase flow modelling. *Computers & Fluids*, 37(7):877–886, 2008.

[54] A. Toutant, M. Chandesris, D. Jamet, and O. Lebaigue. Jump conditions for filtered quantities at an under-resolved discontinuous interface. part 1: Theoretical development. *International journal of Multiphase flow*, 35(12):1100–1118, 2009.

[55] A. Toutant, M. Chandesris, D. Jamet, and O. Lebaigue. Jump conditions for filtered quantities at an under-resolved discontinuous interface. part 2: A priori tests. *International Journal of Multiphase Flow*, 35(12):1119–1129, 2009.

[56] F. X. Trias, D. Folch, A. Gorobets, and A. Oliva. Building proper invariants for eddy-viscosity subgrid-scale models. *Physics of Fluids*, 27(6):065103, 2015.

[57] F. X. Trias, A. Gorobets, M. H. Silvis, R. W. C. P Verstappen, and A. Oliva. A new subgrid characteristic length for turbulence simulations on anisotropic grids. *Physics of Fluids*, 29 (11):115109, 2017.

[58] A. W. Vreman. An eddy-viscosity subgrid-scale model for turbulent shear flow: Algebraic theory and applications. *Physics of fluids*, 16(10):3670–3681, 2004.

[59] B. Vreman. *Direct and large-eddy simulation of the compressible turbulent mixing layer*. PhD thesis, University of Twente, 1995.

[60] B. Vreman, B. Geurts, and H. Kuerten. A priori tests of large eddy simulation of the compressible plane mixing layer. *Journal of Engineering Mathematics*, 29(4):299–327, 1995.

[61] B. Vreman, B. Geurts, and H. Kuerten. Subgrid-modelling in LES of compressible flow. *Applied Scientific Research*, 54(3):191–203, 1995.

[62] A. Weiner and D. Bothe. Advanced subgrid-scale modeling for convection-dominated species transport at fluid interfaces with application to mass transfer from rising bubbles. *Journal of Computational Physics*, 347:261–289, 2017.

[63] A. Yoshizawa. Statistical theory for compressible turbulent shear flows, with the application to subgrid modeling. *Physics of Fluids*, 29(7):2152–2164, 1986.

[64] Z. Zhou, S. Wang, and G. Jin. A structural subgrid-scale model for relative dispersion in large-eddy simulation of isotropic turbulent flows by coupling kinematic simulation with approximate deconvolution method. *Physics of Fluids*, 30(10):105110, 2018.